NUMERICAL CALCULATIONS OF VISCOUS HIGH-ALTITUDE EXHAUST PLUME FLOW FIELDS

Frederick P. Boynton

Wayne State University

Prepared for:

Space and Missile Systems Organization
Advanced Research Projects Agency

December 1970

SAMSO TR 73-106

NUMERICAL CALCULATIONS OF VISCOUS HIGH-ALTITUDE EXHAUST PLUME FLOW FIELDS

by

Frederick P. Boynton

Sponsored by

Advanced Research Projects Agency
Contract No. F04701-69-C-0230
ARPA Order No. 1389
Program Code No. 9E50

Monitored by

Space and Missile Systems Organization
Air Force Systems Command
Norton Air Force Base, California 92409

Research Institute for Engineering Sciences
College of Engineering
Wayne State University
Detroit, Michigan 48202

TABLE OF CONTENTS

UNCLASSIFIED

Security Classification

DOCUMENT CONTROL DATA - R & D

(Security classification of title, body of abstract and indexing annotation must be entered when the overall report is classified)

1. ORIGINATING ACTIVITY (Corporate author)

Wayne State University
Detroit, Michigan 48202.

2a. REPORT SECURITY CLASSIFICATION

UNCLASSIFIED

2b. GROUP

3. REPORT TITLE

Numerical Calculations of Viscous High-Altitude Exhaust Plume Flow Fields

4. DESCRIPTIVE NOTES (Type of report and inclusive dates)

Special Report

5. AUTHOR(S) (First name, middle initial, last name)

Frederick P. Boynton

6. REPORT DATE	7a. TOTAL NO. OF PAGES	7b. NO. OF REFS
December, 1970	~~73~~ 76	14

8a. CONTRACT OR GRANT NO.	9a. ORIGINATOR'S REPORT NUMBER(S)
F04701-69-C-0230	RIES-70-18
b. PROJECT NO. 9E50	
c.	9b. OTHER REPORT NO(S) (Any other numbers that may be assigned)
d.	SAMSO TR 73-106

10. DISTRIBUTION STATEMENT

Approved for public release - distribution unlimited

11. SUPPLEMENTARY NOTES	12. SPONSORING MILITARY ACTIVITY
	Space and Missile Systems Org. Air Force Systems Command Norton A.F.B., California 92409

13. ABSTRACT

This paper describes the results of exhaust plume flow field computations at ionospheric altitudes. Viscous transport, including multicomponent and pressure diffusion, is included in the plume-atmosphere shock layer. The shocks are treated as discontinuities across which the Rankine-Hugoniot relations are applied. The intent of the calculations is to provide detailed composition and temperature distributions in the entire flow from the high temperature bow region to the trailing Mach disc region.

DD FORM 1 NOV 68 1473 REPLACES DD FORM 1473, 1 JAN 68, WHICH IS OBSOLETE FOR ARMY USE.

UNCLASSIFIED

Security Classification

14. KEY WORDS	LINK A		LINK B		LINK C	
	ROLE	WT	ROLE	WT	ROLE	WT
Viscous High-Altitude Flow Fields						
Exhaust Plume						
MULTITUBE						

Figure Captions

1. Distribution of mixture ratio ($\dot{m}_{oxidizer}/\dot{m}_{fuel}$) versus radial distance at the exit plane of the engine.

2. Sketch of the nozzle and undisturbed flow field configurations. The various regions, streamlines, and surfaces are described in the text (pp. 7-12).

3. Streamlines, isotherms, and shocks in the interior and undisturbed exterior flow field near the engine. Smooth temperature curves were obtained by assuming that the temperature in a streamtube is that of its midpoint except for the flow through the Mach disc.

4. Limiting form of the density distribution in the undisturbed external flow field at great distances from the nozzle exit. This is the density profile versus polar angle along a meridian of a spherical surface centered near to the engine exit, where the radius of the sphere $R >> r_e$. A smooth curve is obtained by assuming that the density of a streamtube is that at the tube midpoint, except for the flow through the Mach disc.

5. A replotting in polar coordinates, with a linear radial scale, of the density distribution versus polar angle shown in Figure 4.

6. Flow regimes in the nose region of the plume versus altitude according to the classifications of Probestein and Kemp and of Cheng.

7. Structure of the results of the flow calculation in the outer few streamtubes of the undisturbed flow.

8. Mesh construction for the bow region flow calculation. The dimple in the shock position at the axis results from approximations employed in the mesh construction and is not believed to be meaningful. The actual ratio of streamtube widths on the air side of the shock layer to those on the jet side is much greater than shown here.

9. Jet shock position (from the inviscid Newtonian boundary (NB) calculation), dividing streamline positions (from the inviscid NB calculation and the viscous calculations, bow and supersonic regions) and computed air shock positions after the 1st, 2nd, and 3rd iterations in the bow region calculation. The slip line between the exhausterator gas and the thrust chamber gas is also shown.

10. Viscous layer approximation to the flow field of the plume in the nose region. The vehicle is indicated at the upper left. Isotherms and slip lines between Mach disc and external gas and between turbine (exhausterator) and thrust chamber gas are indicated in the undisturbed flow. Isotherms (°K), jet and air shock positions, and the dividing streamline are shown for the shock layer. The resolution of the calculation prevents precise location of isotherms in the region very near the nose. The air shock position within about 150 meters of the nozzle is faired through the results of the second iteration to the bow region calculation and arbitrarily made convex-forward at the nose; the computed shock location is indicated. Note the large ambient mean free path, indicating that the air shock should be thick in this region with respect to the shock layer as a whole. See next (pp. **30-31**) for further discussion of this point.

11. Viscous layer approximation to the plume flow field in the upstream region (approximately the first second after vehicle passage of the right-hand side of the paper). The station at which air and exhaust mass flows in the mixing layer are equal is indicated. Upstream from this point, most of the shock layer gas came from the exhaust; downstream, most from the atmosphere.

12. Viscous layer approximation to the flow field to 25 km behind the vehicle. Scale height effects should distort outer regions of the aft portions of this flow field. Flow behind the jet-atmosphere Mach disc is approximate. Positions at which the Mach disc would occur according to various steady-flow criteria are indicated.

13. Computed temperature and density profiles along a surface normal to the flow streamlines at a position where $x_{D\,SL}$, the axial distance of the dividing streamline aft of the engine, is zero. The stepwise variation of T and ρ with distance across the surface reflects the resolution of the calculation.

14. Temperature and density profiles at $x_{D\,SL}$ = 100 meters.

15. Mole fraction profiles of exhaust and atmospheric species at $x_{D\,SL}$ = 100 meters. Smooth curves were drawn by assuming that the streamtube compositions were those at the tube midpoints.

16. Temperature and density profiles at $x_{D\,SL}$ = 200 meters.

17. Mole fraction profiles at $x_{D\,SL}$ = 200 meters.

18. Temperature and density profiles at $x_{D\,SL}$ = 500 meters.

19. Mole fraction profiles at $x_{D\,SL}$ = 500 meters.

20. Temperature and density profile at x_{DSL} = 1000 meters

21. Mole fraction profiles at x_{DSL} = 1000 meters.

22. Temperature and density profiles at x_{DSL} = 2000 meters.

23. Mole fraction profiles at x_{DSL} = 2000 meters.

24. Temperature and density profiles at x_{DSL} = 5000 meters.

25. Mole fraction profiles at x_{DSL} = 5000 meters.

26. Temperature and density profiles at x_{DSL} = 10,000 meters.

27. Temperature, pressure and density profiles at x_{DSL} = 25,000 meters. Here the increase in density near the inner side of the shock layer (in this case, the plume axis) is associated not only with cooler temperatures, but also with shock reflection from the axis which is unresolved on the scale of the calculation, but which can be seen in the pressure profile.

28. Mole fraction profiles at x_{DSL} = 25,000 meters. Results for "HC" profiles closer than about 1500 meters to the axis are unreliable because of input error in setting up this portion of the calculation. The effect on other flow variables is negligible.

29. Variation of computed shock layer Knudsen number with radial distance of the dividing streamline from the axis in the forward portion of the plume ($x_{DSL} \leq 1600$ meters).

Introduction

This paper describes the results of exhaust plume flow field computations at ionospheric altitudes. Viscous transport, including multicomponent and pressure diffusion, is included in the plume-atmosphere shock layer. The shocks are treated as discontinuities across which the Rankine-Hugoniot relations are applied. The intent of the calculations is to provide detailed composition and temperature distributions in the entire flow from the high temperature bow region to the trailing Mach disc region.

Effects considered in describing the nozzle and the undisturbed (vacuum) flow field include the distribution of mixture ratio across the injector; an annular shroud of turbine exhaust gases surrounding the thrust chamber exhaust; and the effects of the contour of the reflexed nozzle. The model for the rocket engine used in this study resembles the sustainer engine of the ATLAS vehicle. Wave interactions in the nozzle and near field, caused by the discontinuity in wall curvature a short distance downstream from the throat and by the interaction of the choked turbine gases with the main flow at the nozzle exit, are neglected. The complex shock system induced in the near field by the reflexed section of the wall is included; the near-field Mach disc location and size are determined by the triple-point criterion. The contoured nozzle wall causes the density in the undisturbed flow field at large distances from the nozzle to be greater at angles of 20-30 degrees than on the centerline. The nozzle flow, undisturbed flow, and most of the plume-atmosphere interaction flow were calculated with a Lagrangian finite-difference code (MULTITUBE)[1] which includes multicomponent diffusion. The bow region of the

plume, where the air shock is detached at high altitudes, presents a special problem because of the subsonic flow behind this shock. In these computations, the bow region is treated by a newly developed approximate procedure based on the assumption of uniform streamline curvature and allowing for diffusive transport in the shock layer. This computation is carried downstream until the entire shock layer is supersonic; the remainder of the shock layer is then calculated using the MULTITUBE code. The validity of assuming a distinct shock layer with thin shocks (the viscous layer approximation, in the classification of Probstein and Kemp[2]) is examined in light of the computational results. It is probable that in the high-altitude bow region the maximum temperature behind the air shock will not be reached because of mixing with the plume gases.

COMPUTATIONAL PROCEDURES

The interaction between the exhaust gases and the atmosphere at very high altitudes takes place over a region several orders of magnitude larger than a characteristic engine dimension, and at pressures several orders of magnitude lower than the pressures near the nozzle exit. In these highly expanded flows, the method of characteristics, which is a very useful procedure for calculating plume flow fields at moderate expansions, becomes difficult to apply because the mesh becomes highly elongated and truncation errors become large unless the mesh is continually refined. Approximate procedures (blast wave and force balance theories) give reasonable plume shapes, but do not usually lead to detailed descriptions of the local conditions in the interaction region. Since considerable diffusive transport occurs in the shock layer, it is desirable to include these effects in the calculation. In these calculations, except in the bow region where the flow is subsonic on the atmospheric side of the shock layer, a Langrangian finite-difference procedure was employed. This procedure has been described previously[3] and so only a brief summary of it will be reported here.

The computation begins at a station where the flow is wholly supersonic and where properties are presumed known on a surface normal to the flow streamlines. The flow across this surface is divided into a finite number of streamtubes (not necessarily of identical size). The curvature of the dividing streamlines are evaluated from the known pressures in the adjacent streamtube and the normal momentum equation in difference form:

$$\frac{\delta\varphi_k}{\delta s_k} = \frac{4(2\pi r_k)^j}{(U_k+U_{k+1})} \quad \frac{(P_k - P_{k+1})}{(\dot{m}_k + \dot{m}_{k+1})} ,$$

where by convention the index k identifies both a streamtube and the streamline bounding it on the outside (facing downstream). A new surface is then constructed normal to the extended streamlines, and new streamtube areas are defined where the streamlines and the new surface intersect. From these areas and the one-dimensional conservation equations for mass, momentum, and energy, the state properties of the flow in each streamtube at the new surface are determined. In inviscid shock-free flow, with no chemical reaction, the conservation laws take the form:

$$\delta \mathring{m}_k = \delta S_k = \delta H_k = 0.$$

In viscous flows, terms must be added to account for transport by viscous effects; in this work, only transport normal to the flow direction is allowed, an approximation valid for mixing layers where gradients along the flow are much smaller than those across it. The calculation marches downstream in this fashion until the entire region of intersect has been covered.

Boundary conditions must be specified at each edge of the flow; these can take the following forms:

a) a surface whose position is known (including an axis of symmetry),

b) a specified pressure acting on the bounding stream, or

c) a shock propagating into a flow of known properties.

A rather wide class of problems can be treated, subject to the essential restriction that the flow within the region of the calculation be supersonic. Thus although the technique was originally developed for computing the highly expanded external flow, it can also be used for determination of the nozzle and external near fields.

The principal advantages of the technique in comparison to other numerical procedures are its ability to satisfy rigorously the integral conservation laws for mass and total enthalpy (subject however to roundoff errors, convergence errors as in the iterative state property calculations when the specific heat is temperature-dependent, and interpolation errors crossing shocks when the upstream flow is not uniform) and the ease of mesh construction at high Mach numbers, where the streamline curvature becomes small. Its principal disadvantage, which it shares with most other Langrangian and Eulerian techniques, is that it does not rigorously preserve influence regions, and thus wave interactions are not treated exactly. This property causes some difficulty in handling the flow converging toward an axis, as we shall see later.

The restriction of this technique to wholly supersonic flows requires us to use other procedures to compute the flows in subsonic regions, such as the air side of the shock layer in the bow region and the flow immediately downstream from subsonic regions. We have used approximate procedures for these regions, and these procedures will be discussed in later sections.

INTERNAL AND UNDISTURBED EXTERNAL FLOW

The contour of the nozzle wall downstream from the throat consists of three separate sections joined smoothly together. Immediately downstream from the throat, a short circular-arc section turns the adjacent flow to an angle of about 30°, where it enters an approximately conical section. This conical section expands the flow to a geometrical area ratio of , where it then joins to a parabolic reflexed section which completes the expansion to an area ratio of 25 and turns the wall flow back parallel to the axis. Previous calculations of conditions at the exit-plane of high-area ratio nozzles have shown them to be insensitive to the details of the flow in the throat region. Accordingly, we have assumed that the flow is source-like with constant pressure near the end of the conical section, and use this as the initial condition.

We also require a specification of the chemical composition of the flow. The mixture ratio distribution is determined after a plot of mixture ratio versus radial distance at the exit plane of the sustainer engine (furnished by Aerospace Corporation)[4], shown in Figure 1. Using a previously computed distribution of state pressure at the exit plane of this engine, the information on the plot was converted to mixture ratio versus mass flow, and then to the mixture ratio distribution on the constant-pressure initial surface. To determine the initial temperature, we assumed that all chemical reactions in each streamtube froze suddenly at a pressure slightly below the throat pressure. Composition and temperature in each streamtube were determined by interpolating between results of one-dimensional calculations[4] for the sustainer at its nominal operating mixture ratio and for the vernier engine at a mixture ratio of 1.8. The flow was assumed to consist of H_2, H_2O, CO, and CO_2, and the small amounts of other species present according to the performance calculations

were neglected. The heat capacities of the species as fractions of temperature were determined from a 3rd-order polynominal fit to the JANAF tabulations.

It proved convenient to carry out the flow calculations in several steps. The primary reason for this is that shocks are treated as boundary conditions and the program does not include the complex logic required to recognize and include a shock as an internal discontinuity. The various flow regions and the streamlines and joining surfaces referenced in the following discussion are shown schematically in Figure 2.

Step 1: Conditions in an initially source-like flow beginning at the initial surface are computed. Boundary conditions are on one side the symmetry axis, and on the other side the conical wall section and its downstream extension. The calculation of this flow is continued downstream to a point well beyond the expected position of the near-field Mach disc. Most of this flow is swallowed by the nozzle-induced shock system; the part which is not swallowed is Region 1 of Figure 2. This flow remains essentially source-like, with small deviations entering because of the differences in thermal properties along the different streamlines.

Step 2: Conditions in the flow near the reflexed section of the nozzle wall are computed down to the nozzle lip. Boundary conditions on one side are an analytical fit to the wall contour, and on the other a shock propagating into and ingesting the flow computed in Step 1. This flow constitutes a portion of Region 2 in Figure 2. The shock begins as a Mach wave at the junction of the conical and reflexed sections and remains weak throughout the internal flow. The pressure in the "shocked" flow increases monotonically toward the wall; the temperature passes through a maximum because of the lower total enthalpy of

the relatively rich gas near the wall.

Step 3: The exhausterator flow is added to the calculation at the nozzle lip and the calculation is continued into the external flow. Properties and composition of the turbine exhaust are essentially taken from unpublished data supplied by Rocketdyne. The gas is assumed to consist of H_2, H_2O, CO, CO_2, and a mixture of other substances, including unburned and partially oxidized species, which for simplicity's sake is treated as a single hydrocarbon with a molecular weight of 70 and transport and thermal properties similar to pentane. The turbine gas is assumed to be choked at the exhausterator exit; it is actually necessary to assume that the gas velocity at the exit is slightly supersonic in order to apply the marching procedure. The exhausterator pressure is taken equal to the pressure in the thrust chamber streamtube adjacent to the wall at the end of the nozzle, and the flow direction is parallel to the axis. In marching downstream from the exit, a rather low resolution is used initially to describe the expansion of the turbine gas and the outer thrust chamber fluid, because of restrictions imposed by the way the computer code adds new streamtubes at the shock. The flow a few tubes inward from the boundary (inside streamline "A" of Figure 2) is essentially unaffected by the resolution employed in treating the flow outside it. Boundary conditions are zero pressure outside the flow, and a shock propagating into the Region 1 flow on the inside. The calculation is carried downstream until the shock intercepts the axis. The shock is found to turn rather abruptly toward the axis shortly downstream from the nozzle exit. The shock is obviously rather suddenly reinforced by compression waves emanating from the downstream part of the reflexed wall section. Because of a peculiarity of the computer code, the temperature downstream of the region of abrupt turning of the shock tends to be higher than the temperature on either side, this is not expected on physical grounds, and must be considered

an artifact of the calculation.

Step 4: The position and size of the Mach disc are determined according to the procedure of Bowyer, D'Attore, and Yoshihara[5] (triple-point calculation assuming that the Mach disc is normal to the flow). The position thus determined is close to that which would have resulted from applying the procedure of Eastman and Radtke[6] (minimum static pressure behind the incoming shock). Adamson's procedure[7] (ambient pressure behind the Mach disc) is not applicable, since P_∞ zero, and we were not acquainted with the method of A bett[8] (force the flow behind the disc to pass smoothly through a throat, which is the most reasonable procedure outside of a time-dependent or relaxation calculation) at the time the calculation was done. The Mach disc found is rather large; about 2% of the thrust chamber mass flow passes through it.

Step 5: The flow outside the Mach disc is extended downstream from the point at which the calculation of Step 3 was halted. A number of streamtubes which would have passed through the reflected shock are dropped from the calculation. The external boundary condition is still zero pressure, and the internal boundary condition (at streamline "B" of Figure 2) is a prescribed (low) pressure. The (virtual) behavior of streamline "B" downstream is sketched in Figure 2. We are not concerned with the behavior of the flow near the internal boundary, since this region of the flow is eventually swallowed by the reflected shock. Our main concern is that the influence of the boundary on the region of the flow where the reflected shock lies be minimal.

Step 6: The expanding flow near the nozzle lip is recomputed, using a resolution adequate to describe the expansion down to pressures expected in the interaction region. The position of streamline "A", determined from the calculations of Step 3, is

assumed fixed, according to our earlier remarks concerning the effects of resolution near the edge of the flow on the results a few streamtubes inside the edge. This streamline is used as the inner boundary of the flow in Region 3, with the outer boundary at zero pressure. In such a calculation, the outermost streamline carried in the calculation never reaches the computed limiting angle of the Prandtl-Meyer expansion about the lip, but approaches it more closely as the initial streamtube width at the edge of the flow is made smaller. There is a practical limit to the resolution employable, and thus to the accuracy of the calculation in the vicinity of the limiting line (taken as that for the expansion from the assumed slightly supersonic initial condition). We have not found this to be a significant limitation on describing the interaction with the atmosphere under conditions of interest in a continuum calculation.

Step 7: At a convenient location, the flows computed in Steps 5 and 6 are combined along a surface normal to the streamlines in the two calculations (joining surface 1 of Figure 2). The flow outside streamline "A" in the low-resolution calculation is replaced by the high-resolution calculation of Step 6. The flows thus joined appear to exhibit no peculiarities, as we should expect if the flow at and inside streamline "A" is only slightly affected by external resolution. The combined flows are then continued downstream from joining surface 1. In practice, the calculation was halted when it appeared that the disturbance introduced from the inner boundary (streamline "B") was beginning to affect the region near the expected position of the reflected shock from the Mach disc. The choice of internal boundary pressure in this calculation could have been better chosen to permit a further extension downstream of the flow outside the reflected shock. A still more reasonable approach might have been the systematic dropping of streamlines on the internal side of the calculation,

assuming that some generally applicable procedure could be worked out. As it is, the limitation in the distance downstream to which the Region 2 flow was carried in this caluclation limits the distance to which a finite-strength shock can be propagated into this flow (about 4 meters downstream from the nozzle exit). This deficiency, though not qualitatively serious, eventually introduces some wiggles into the far-field density distribution.

Step 8: The calculation of the flow downstream from the Mach disc is begun, starting with a single streamtube whose properties are those behind the reflected shock at the triple point. The outer boundary condition is a shock propagating into the previously calculated flow in Region 2. The inner boundary is taken as a cylindrical surface parallel to the axis; this surface is intended to simulate, in very crude fashion, the slip line between the gas passing inside and outside the triple point. The calculation is continued downstream (the code adds more streamtubes as the shock ingests the upstream flow) until the pressure in the streamtube adjacent to the inner boundary falls to that at which the Mach disc gases, after passing through a throat, have the same one-dimensional area as the Mach disc itself but have a supersonic velocity.

Step 9: The flow behind the Mach disc is added to the flow behind the reflected shock (at joining surface 2 of Figure 2). Its pressure is the pressure at which it reexpands to its initial area, and the flow angle of the streamline bounding it is chosen arbitrarily to be one-half the flow angle of the next outer streamline. The calculation is then continued downstream, with the axis as one boundary and the reflected shock as the other, far as the calculation of Step 7 permits. The junction of the Mach disc flow with the remainder of the Region 4 flow appears to have been made smoothly, since no pressure oscillations occur in the subsequent calculations nor does the shock appear to take any sudden twists.

Step 10: At joining surface 3, the Region 2 and Region 4 flows are combined along a normal surface, with the Region 4 flow replacing the inner portion of the Region 2 flow. From this point on, dissipation in the reflected shock is neglected, and the shock is replaced by its isentropic approximation. The pressure rise across the shock at this point is about a factor of 2. Some pressure oscillations ($\Delta P/P \approx 10\%$) are observed in the solution immediately downstream from this point. They appear not to be completely damped, but seem to be frozen into the far field pattern of density distribution. The computation can be carried as far downstream from this joining surface as one cares to go. We ran the results 100 km downstream in 2 minutes, 36 seconds on a Univac 1108.

The results of the calculations in the region near the nozzle exit are shown in Figure 3. Here we have plotted various streamlines, isotherms, and shocks developed in the course of the calculation. A few features of this plot require further comment:

The turbine gas flow expands to very large angles because of its low Mach number. If this gas were not present, its place would be taken by the gas from the thrust chamber wall boundary layer, and densities at large angles would be lower. The turbine gas confines the thrust chamber gas, and prevents it from expanding as far as it would if the turbine products were not present. It is not necessary to consider the wall boundary layer when the main flow is surrounded by a shroud of low-Mach number gas, unless one wants great detail in the region near the dividing streamline between the main and turbine flows. In that case, one should also include mixing of the two flows, and we believe that in most cases the mixing layer would soon swallow the wall boundary layer.

The Mach disc formed in these calculations is large. Several years ago, computations were performed by D'Attore[9] of the flow

near the Mach disc downstream from the nozzle of a simulated Atlas sustainer engine, assuming that reservoir conditions were the same on all streamlines and that the specific heat of the gas was 1.225. These computations showed a much smaller disc than that found here, and agreed well with schlieren photographs of the shock system of a 100-lb. thrust model engine. The discrepancy between the current calculations and the earlier work could either be real, or could be an error in our calculations. On the one hand, it is possible to rationalize the occurrence of a large Mach disc by noting that the flow near the centerline has a high mixture ratio and is thus hotter, less dense, and at a somewhat lower Mach number than its counterpart in a flow with uniform mixture ratio. These conditions favor a large disc, since the internal flow (behind the intercepting shock) is less able to support a pressure gradient and collapses faster as it is squeezed by the outer flow. On the other hand, the failure of the calculation to preserve wave interactions makes it difficult to describe accurately the wave effects in the flow behind the intercepting shock, and the calculation does not handle quite properly the rapid coalescence of the nozzle compression waves into the strong intercepting shock. Thus while it is plausible that the Mach disc should be somewhat larger than that found in earlier work, there also may be some computational error affecting its size. We would welcome a separate computation of this part of the flow field by a different numerical procedure.

The flow at large distances from the nozzle eventually becomes self-similar as the ratio of pressure to inertial forces approaches zero. The limiting form of the density distribution is shown in Figure 4. The wiggles at $\theta \approx 30$ to 40 degrees are partly due to variations in total temperature and molecular weight induced by mixture ratio variations in the chamber, and are partly due to oscillations in the numerical solution caused by the somewhat premature junction of the flow behind the reflected

shock with the flow at larger angles (at joining surface 3 of Figure 2). The nozzle-induced shock system produces a density defect along the centerline of the flow; this defect is shown rather dramatically in Figure 5, which is a polar coordinate plot of density versus angle in the undisturbed far field. The undisturbed plume has a "hole in the middle" because of the non-ideality of the nozzle.

INTERACTION OF THE EXHAUST AND THE ATMOSPHERE

The calculations reported here were all performed using a computational procedure based on the continuum equation of motion. Before describing the calculations and the results, a few remarks on the validity and limits of continuum models at high altitude appear in order.

The generally accepted criterion for the validity of a continuum calculation is that the local mean free path in the region of interest be somewhat smaller than the distance over which some desired property of the flow changes significantly. This criterion is a bit vague, and the meanings of "somewhat smaller" and "significantly" have to be adjusted to fit particular situations and the questions being asked of the results. In the case of the exhaust plume, a pertinent local dimension is the width of the shock layer or some fair-sized fraction of this width. We should expect that the local velocity, enthalpy, and density would be reasonably well described by a continuum model when $\lambda < \rho/\nabla\rho$. It is difficult to apply this criterion to a flow one has not yet computed; fortunately, procedures have been evolved which help one to decide under what conditions his computations may be expected to be reliable.

At the altitudes of interest, the dividing streamline (that is, the streamline which bounds a mass flow equal to the jet flow) assumes a large angle near the nozzle. The external flow perceives this part of the exhaust flow as a blunted body, and a detatched shock is set up in the external stream. The dynamic pressure of the atmosphere forces the dividing streamline back toward the axis as the jet flow expands and its pressure decreases. The curvature of the dividing

streamline defines a nose radius for the plume equivalent to that of a blunt body. This radius can be determined empirically, as from photographs of high-altitude plumes, or by approximate computational procedures invoking a force balance between the internal and external streams, such as blast wave theory. Having the nose radius and the free-stream conditions, one can make use of the procedures developed for blunt-body flows to determine the kind of treatment he must apply to a specific problem.

The nose region involves only a very small part of the jet and atmospheric mass flow which eventually gets incorporated into the shock layer, and its dimensions are much smaller than those of the shock layer further downstream. We therefore expect that if continuum procedures break down, they will do so first in the nose region. It is quite possible to have a plume in which the extreme forward part of the interaction region does not follow continuum laws while the downstream portions of the shock layer can be well described by a continuum calculation. The problem of supersonic flow near the leading edge of a flat plate provides a qualitative analogy.

In Figure 6 we show the expected behavior of the nose region of the plume from the sustainer engine as a function of conditions along a typical trajectory. This curve, taken from a report by Thomson[10] shows the expected passage of the plume through the various flow regimes identified by Probstein and Kemp[3] and by Cheng.[11] The classification schemes are outlined in Table I. The nose radius of the plume as a function of altitude was determined from photographs presented by Rosenberg.[12]

Our computational procedures, which assume that shock waves are thin and allow a pressure gradient normal to the flow in a region of mixing, describe flows in the viscous layer regime. On the basis of Figure 6, we expect them to be valid

at altitudes up to about 140 km In this report we show the results of calculations at 140 km. We should expect to find some signs of incipient breakdown of our assumptions in the nose region, and to find that they remain reasonable downstream from the nose. In general, the results of the calculations confirm our expectations. We have carried the computations thus far down to the region of the plume-atmosphere Mach disc. In subsequent work we plan to extend these calculations further downstream, toward the region of pressure equilibration (the far-field trail), and to calculate the flow at a higher and a lower altitude.

The calculations performed here were done in three separate steps. First, the positions of the jet shock and the dividing streamline are located by assuming that the atmospheric pressure exerts its Newtonian pressure on the dividing streamline. Second, the flow in the bow region is computed assuming that the jet shock is fixed and that the curvature is constant across the flow, and allowing multicomponent diffusion of the jet and atmosphere gases. Third, the bow region calculation is halted at a position where the entire flow is supersonic and the calculation is continued with a shock boundary condition on either side. The first and third calculations are performed with the MULTITUBE code, the second with a newly developed code (BOWTUBE) which is similar to MULTITUBE in its treatment of diffusive processes. In all the interaction regions, we assume that translational and rotational degrees of freedom are rapidly equilibrated but that vibrational electronic, and chemical modes remain frozen. The specific heat at constant volume is thus 5/2R, 7/2R, or 4R for a monatomic, diatomic or linear polyatomic, or non-linear polyatomic species respectively.

Newtonian Boundary Calculations: The calculation is initiated at a point where the local static pressure in the jet is equal to the Newtonian pressure of the atmosphere. One jet streamtube is used at the initial surface. The atmospheric Newtonian pressure (equal to ρ_∞/u_∞^2 for dividing streamline flow angle greater than 90°) acts on the external boundary. The internal boundary is a shock propagation into and ingesting the undisturbed jet flow. This calculation is continued downstream until the external flow has turned the dividing streamline through a large enough angle (back toward the plume axis) so that an inviscid flow on the air side of the shock layer would be entirely supersonic.

The principal difficulty with this calculation is getting it started in the right place and in the right direction. If it is not started correctly, large oscillations are present in the solution near the starting point as the shock layer alternately overshoots and undershoots its correct position. At high initial shock layer Mach numbers, the flow is stiff and the oscillations can be very large if the choice of initial point and direction are particularly bad. These oscillations are eventually damped as more mass is added to the flow, but they can result in highly unrealistic behavior of the jet shock and dividing streamline.

At low altitudes, one can usually get good solutions by starting the shock layer calculation at the angle where the atmosphere's Newtonian pressure equals the pressure in the jet expanded to that angle in an ordinary Prandtl-Meyer expansion. The jet shock angle is then the Mach angle, and the calculation proceeds without difficulty. At high altitudes, two other considerations enter: First, one does not want to initiate the calculation too close to the nozzle because the jet shock layer is extremely thin at this position and it takes a fairly long time to march away from the initial point to regions of more

interest. Second, the way in which the vacuum expansion calculation does the large-angle flow often results in the Prandtl-Meyer line at the atmospheric Newtonian pressure's lying outside the computed vacuum flow until some distance away from the nozzle. Recall that the requirement of finite resolution in the outer few streamtubes of the vacuum expansion results in the outer streamline's turning with a finite radius and that it never quite reaches the true limiting angle. As a consequence, the Prandtl-Meyer line calculated in the usual way may not penetrate the calculated vacuum flow until the flow is far enough from the axis that radial dilation begins to affect the local properties. This situation is shown in Figure 7, where the departure of the locus at which the local static pressure is the undisturbed flow is equal to the atmospheric impact pressure from the initial Prandtl-Meyer line is sketched along with representative streamline positions.

We found that starting the calculation a moderate distance (here about 5 meters) from the axis on the line where $P = \rho_\infty u_\infty^2$, giving the initial streamtube a pressure of $\rho_\infty u_\infty^2$ and a direction along the locus of constant pressure, resulted in a relatively smooth calculation everywhere. These starting conditions are not quite correct, and the resulting solution is found to oscillate slightly ($\Delta P/P \sim 20\%$) for several meters downstream. However, the corresponding "wandering" of the streamline is hardly noticeable, and the oscillations appear to be damped quickly enough that the flow at 10-15 meters or farther from the axis is essentially unaffected. Our computations do not in any case provide a realistic description of the flow within 10-15 meters of the nozzle axis in the nose region. Since this is a very small part of the plume (and even of its blunt portion), we do not consider this a significant difficulty.

Bow Region Calculations: In the forward portions of the shock layer at this altitude, the atmospheric shock is detatched and the flow immediately behind it (according to the Rankine-Hugoniot relations) is subsonic. This flow mixes rapidly with the supersonic jet flow, and the equations describing the resulting flow field are of a mixed character. In principle, one could solve for the flow field as the limit of an unsteady problem using the complete Navier-Stokes equations; this approach easily allows shocks of finite thickness and would be extended into the merged layer regime. Sample computations indicated that such calculations would be lengthy if a mesh was used which allowed good resolution of the rather sharp density gradients expected on the jet side of the shock layer. (The jet gases are cold and dense and the mean free path on the jet side of the shock layer is up to 50 - 100 times smaller than that on the air side.) We therefore adopted a different procedure which is approximate, but which should yield reasonable results for conditions within the mixing region a few major steps downstream from the starging point.

In these calculations we assume that the jet and air shocks are sharp discontinuities and that the ordinary Rankine-Hugoniot relations apply across them. We also assume that the pressure gradient normal to the inner boundary can be found by assuming constant streamline curvature across the flow. (This assumption is clearly wrong in regions of near-stagnation, but the errors introduced should be moderate since the pressure gradients are not large in any case.) The jet shock position determined from the Newtonian boundary calculation is taken as fixed; in support of this assumption, we note that the relatively steep gradients in the undisturbed jet flow

make it difficult to displace the shock layer on the jet side without the resulting higher (lower) pressure's tending to push (pull) it back to its original position.

The calculation is initiated at the same station at which the Newtonian boundary calculation is begun. Two streamtubes are taken crossing a surface perpendicular to the jet flow direction: the initial jet stream and an air streamtube. The width of the air streamtube is calculated by assuming that its properties are those behind a normal shock and balancing the mass flow between the outer boundary and the axis with that across the initial surface. The inner boundary is the streamline determined in the Newtonian boundary calculation; the outer boundary is developed during the calculation by mass conservation. The calculation marches downstream across successive surfaces drawn perpendicular to the inner streamline boundary. Diffusive transport is allowed across internal streamlines, but not across the bounding streamlines. At each surface the flow across it is constructed according to the following set of difference equations, where k identifies both a streamline and the streamtube which it bounds and ℓ identifies the surface:

Global continuity: $\overset{\circ}{m}_k = \text{constant}$

Streamwise momentum: $\overset{\circ}{m}_k(u_{k,\ell} - u_{k,\ell-1}) + \tfrac{1}{2}(A_{k,\ell} + A_{k,\ell-1}) \cdot (P_{k,\ell} - P_{k,\ell-1}) = 2\pi\Delta_k \{ r_k \tau_k \delta s_k \}$

Normal momentum: $(P_{k,\ell} - P_{k-1,\ell}) = K_\ell (u_{k,\ell} + u_{k-1,\ell}) \cdot (\overset{\circ}{m}_k + \overset{\circ}{m}_{k-1})/(8\pi r_{k,\ell})$

$$\text{Energy:}\quad \mathring{m}_k(h_{k,\ell} - h_{k,\ell-1} + \tfrac{1}{2}u_{k,\ell}^2 - \tfrac{1}{2}u_{k,\ell-1}^2) = 2\pi\Delta_k\{r_k \cdot (q_k + \left[\tfrac{1}{2}(u_k^2 + u_{k+1}^2)\right]^{\frac{1}{2}}\tau_k + \sum_i \bar{h}_{i,j}J_{i,j})\delta s_k\}$$

$$\text{Species continuity:}\quad \mathring{m}_k(c_{i,k,\ell} - c_{i,k,\ell-1}) = 2\pi\Delta_k\{r_k J_{i,k}\delta s\}$$

The operator Δ_k takes the difference in the term in braces across the kth streamtube. The pressure at the inner boundary is determined from the Newtonian boundary calculation, and K_ℓ is the curvature of the inner boundary.

The mesh is constructed by stepping a chosen distance (consistent with the stability limitation, since this is an explicit difference scheme) along the inner boundary and solving for the streamtube areas and state properties along a line normal to the inner boundary using the pressure generated from the normal momentum equation, the conservation laws, and the equation of state for a mixture of perfect gases. In developing the difference equations, we have assumed that this line is essentially normal to the flow direction. The stepping distance is determined from

$$\delta s = \frac{\alpha}{2}\ Re_k\ F_k\ \delta y_k$$

where

$$F_k = \min\{1, Pr_k, Sc_{ij,k(i\le l\le N, j\ne i)}\},$$

α is some number less than one, Re_k is the streamtube's Reynolds number, δy_k its width, and Pr and Sc the local Prandtl and Schmidt numbers. A second-order stepping scheme is used, with the fluxes for the first trial at the new surface calculated at the old surface and the fluxes for the second trial the averages of those at the old and new surfaces.

A multicomponent diffusion scheme, including pressure and thermal diffusion, is used in calculating the species fluxes. The subroutines calculating the transport are identical to those from MULTITUBE. The flux laws for diffusion are the Stefan-Maxwell equations

$$\sum_j \frac{x_i x_j}{\rho D_{ij}} \left[\frac{J_j}{c_j} - \frac{J_i}{c_i}\right] = \frac{\partial x_i}{\partial y} + (x_i - c_i) \frac{\partial \ell n P}{\partial y}$$

$$- \frac{\partial \ell n T}{\partial y} \sum_j \frac{x_i x_j}{\rho D_{ij}} \left[\frac{D_j^T}{c_j} - \frac{D_i^T}{c_i}\right], \quad (1 \le i \le N).$$

This set of N-1 linearly independent equations, together with the condition that no net transfer of mass occurs across a streamline,

$$\sum_j J_j = 0,$$

can be solved for the species fluxes. Further details of the diffusion calculation can be found in Reference . In the calculations reported here, thermal diffusion was neglected, since previous calculations indicated that its contribution to the total flux was considerably smaller than those of either ordinary or pressure diffusion.

The calculation proceeds downstream in this fashion until it reaches the surface at which the Newtonian boundary calculation added another streamtube to the flow. At this point, new streamtubes are added on both the jet and air sides. The properties of the new jet tube are taken from the Newtonian boundary calculation. The properties in the new air tube are those behind a shock at the average angle of the inner boundary between this station and the point at which the last previous

jet tube was added to the calculation. If this angle is greater than 90°, a normal shock is assumed. The width of the new shock tube is determined by mass conservation. The computation then continues to march downstream, now carrying two more streamtubes in the calculation. New streamtubes are added on each side in this fashion at each point at which the Newtonian boundary calculation added a new tube. The mesh construction is shown in Figure 8.

Although the above calculation tacitly assumes that the air shock lies very close to the Newtonian boundary, the low density of the air side of the shock layer and the rapid growth of the jet side as it is heated by the air combine to push the air shock away from the original boundary. To take this effect into account, we redo the entire bow region calculation. This time, when adding a new air streamtube to the flow, we calculate its properties by assuming that the shock angle is that found in the previous calculation during the mesh construction there. Presumably, we could carry the calculation through further iterations; in this work, we cut it off in the second iteration because it appeared that in higher iterations an unstable inflection in the computed air shock was developing in the region where the angle of the dividing streamline is about 90°. (This instability may be removable by altering the mesh construction.) Further iterations would tend to move the air shock somewhat farther away from the jet shock.

The computed air shock has a pronounced dimple near the axis. Although one might argue that a slight dimple could be produced by rapid entrainment in the mixing layer, we regard the dimple as an artifact of our mesh construction and believe that the true air shock position near the axis lies

considerably upstream from where the computer puts it. This would require that the air streamtubes just inside the shock be considerably wider, which in turn requires a higher pressure and lower velocity. These requirements do not seem unreasonable, since we expect this region to involve near-stagnation and partial reversal of the air flow. It should be possible to improve the calculations to allow construction of a shock whose angle is never greater than 90° (based perhaps on the farthest upstream location found for the shock in the previous interation), and we plan to investigate this possibility in subsequent calculations.

The BOWTUBE code was used to calculate flow in the shock layer downstream to the point where the Mach number in the outermost stream tube was about 1.35. The sonic line in these calculations extends furthest downstream near the air shock, because of the swallowing of higher-entropy gas near the dividing streamline by the mixing region.

Fully Supersonic Region Calculations: In the region downstream from the nose, the plume flow is wholly supersonic. We apply the MULTITUBE code to this region, starting at the last surface calculated by BOWTUBE. No a priori assumptions about streamline curvature or pressure gradients are made. Multicomponent diffusion (including pressure diffusion) is allowed across the shock layer. Boundary conditions are shocks propagating into the undisturbed jet and atmosphere. These calculations were carried down to where the jet shock is calculated to reach the axis.

In all the above work, the properties of the atmosphere are those of CIRA model 5 ($\overline{F}_{10.7} = 150 \times 10^{-22}$ w/m^2 cps, mean level of solar activity) at hour 14 (exospheric temperature 1417°K).[13] At this altitude the effect of variations in

atmospheric properties on conditions in most of the plume are not great, although some changes in plume size and far-field temperatures are to be expected. Vehicle velocity at this altitude was taken from a representative trajectory supplied by Aerospace Corporation.[4] Important atmospheric properties are shown in Table II. In order to simplify the diffusion calculations, we have treated O_2 and N_2 as a single species.

Table II

Atmospheric Parameters

Ambient pressure	$P = 7.9 \times 10^{-9}$ atm
Ambient temperature	$T = 638°K$
Ambient composition	$n_{N_2} = 6.09 \times 10^{10}$ cm^{-3}
	$n_{O_2} = 9.50 \times 10^{9}$ cm^{-3}
	$n_O = 2.02 \times 10^{10}$ cm^{-3}
Vehicle velocity	$v_M = 3.7$ km/sec
Mach number	$M = 6.87$

Results of the Calculations: Figure 9 shows the calculated position of the jet shock, dividing streamline, and dividing streamline between the exhausterator and thrust chamber gas according to the Newtonian boundary computation (carried about 400 meters downstream from the exit). A small portion of the jet flow, composed entirely of exhausterator (turbine) gas, does go "forward" at this altitude; however, beyond about 40 meters from the plume axis, the entire shock layer is going "aft" (in the general direction of the vehicle thrust vector) and beyond about 60 meters the whole plume, including the undisturbed flow, goes aft. For comparison,

the dividing streamline position obtained in the bow region calculation (iteration 2) and its downstream extension in the supersonic calculation are also shown in Figure 9. Viscous displacement effects cause this streamline to lie well outward from where it would fall in a wholly inviscid calculation, expecially once the flow is going aft. Figure 9 also includes the calculated air shock positions in the first three iterations of the bow region calculation. The instability developing in the third iteration between 60 and 120 meters from the axis is quite evident, as is the fact that continued iteration produces a relatively small adjustment of the shock position.

Figures 10 through 12 show shock and dividing streamline positions, together with selected isotherms, in the plume on a progressively larger scale. The vehicle is shown for comparison near the origin in Figure 10. Calculated temperatures in the air side of the shock layer exceed 6000°K in the nose region; the low resolution of the calculation here makes it difficult to trace isotherm positions accurately very close to the nose. We show in Figure 10 both the calculated air shock position in the nose region (iteration 2) and a smoothed curve drawn through it, representing a hypothesized actual shock. Appreciable shock heating of the jet gas entering the shock layer (all exhausterator gas until about 150 meters behind the vehicle) occurs. Temperatures in the vicinity of the turbine-thrust chamber slip line may be somewhat high because the interpolation for properties upstream from the shock allows some improper mixing of these two flows. The flow near the centerline, which passed through the nozzle-induced Mach disc, stays warm for about 100 meters downstream from the exit. The two calculations, BOWTUBE and MULTITUBE, join together reasonably smoothly, although there is some adjustment of the position

of the air shock a short distance downstream from the junction line.

The further development of the flow is for the most part unremarkable until the jet shock begins to converge on the axis. The peninsula-like behavior of the isotherms in Figure 11 is caused by the cooling of atmospheric gas as it mixes with jet gas. Figure 12 shows that the plume is essentially a slender body with a small blunted nose, as Thomson has previously pointed out. One slightly disturbing feature of the calculation is that by the time the jet shock gets back to the axis, the total exhaust mass flow and the mass flows of all the exhaust species outside it are computed to be slightly ($\sim$10%) larger than the values for the undisturbed flow. This difference is most probably a consequence of having to interpolate the computed undisturbed flow in order to obtain properties upstream from the shock at a given point. (We do not have this problem with species coming from the atmosphere.) The errors thus introduced are probably small. Nonetheless, one of the attractive features of the difference scheme is that it does conserve mass flow in a particular domain, and it would be desirable to try to eliminate this unphysical aggrandizement of the shock layer if possible.

At about the time that the jet shock begins to turn back toward the axis, it crosses the slip line between the gas passing through the nozzle-induced Mach disc and that passing outside it. The Mach disc gas is less dense than the surrounding gas, and one might expect the jet shock to exhibit signs of rapid collapse in this region. From our results, it appears that the jet shock continues to approach the axis in a smooth manner and at a moderate angle. The rationalization of this behavior is that the shock layer flow is hypersonic and therefore rather stiff. (Mach numbers across the layer 10 km aft

of the vehicle range from 11 on the inside to 5.5 on the outside.) Although the pressure downstream of the jet shock is falling rapidly, the flow farther out in the shock layer is slow to respond because the inertial forces are large with respect to the pressure forces.

The three "steady-state" procedures for locating the Mach disc in the far field give drastically different results for the disc position and size. The criterion of Adamson and Nicholls[7] would result in a large disc ($r_D \approx 1$ km) about 11 km aft of the vehicle; that of Eastman and Radtke[6] a disc of 300 m radius at about 14.4 km; that of Bowyer, D'Attore and Yoshihara[5] a very small disc very close to where the jet shock is calculated to reach the axis at 15.4 km. aft of the vehicle. We cannot resolve this discrepancy without further computations (as, for example, in Abbett's work) and the question appears somewhat academic when we recognize that the mean free path in the undisturbed gas at x = 13 km is greater than 1 km, so that the triple-point is not small on the scale of the disc. The positions at which applying the above three criteria would place the Mach disc are indicated on Figure 12.

Several profiles of temperature, density, and composition variations across the shock layer are shown in Figures 13 through 28. The temperature and density are shown in the stepwise-varying fashion resulting from our solution, with the actual mesh size; this representation would be too confusing for the composition profiles, and for these we show smooth curves of mole fraction versus distance assuming that in each tube the calculated mole fraction is associated with the midpoint. The abscissa is a line normal to the flow direction from the first to the last streamline carried in the calculations. These end points are usually not the shock locations because the

shock is always growing away from the calculated flow except at the station at which a new streamtube is added to the calculation. The figures show data at successive axial positions aft from the nozzle throat along the dividing streamline. The data at $x_{DSL} = 0$ are from the bow region calculation, those at $x_{DSL} = 100$ are from the supersonic calculation shortly after it takes over from the bow calculation, and the rest from the supersonic calculation.

Diffusion in the bow region is rapid. At $x_{DSL} = 0$, the temperature and composition profiles within the internal region are fairly flat. The outer tubes are newly added jet and air streamtubes. Conditions in these tubes appear out of line with those in the internal tubes. The mean free path behind the bow shock in this region is about 3.5 meters, which is about equal to the width of the outermost tube; in the next tube it is about 1 meter, or about equal to the width of that tube. The ratio of λ to δy, the tube width, decreases as we move toward the jet side. The jet shock thickness (determined from the maximum density gradient in the shock) should be about 1 meter at this station, and the air shock thickness about 10 meters. Clearly, neither shock is thin in relation to the scale of computed gradients in the adjacent internal flow, although the jet shock is thinner on this scale by comparison to the air shock. It therefore seems highly likely that neither the maximum temperature nor the maximum density found in the calculation are actually attained in the shock layer, which at this station is in the "incipient merged layer" flow regime. Conditions in the internal region (which here comprises the exhaust-air mixing region) are probably reasonably accurately described in terms of properties versus mass flow, which is the relevant question for analyses of shock layer chemistry

involving exhaust-air interactions. However, even here one should ask more detailed questions about molecular velocity distributions and their adjustment to local equilibrium conditions.

At x = 100 m (Figures 14 and 15), the scale of gradients in the shock layer is larger compared to the mean free path, and we conclude that here the viscous layer description is appropriate except at the shocks themselves. Further downstream it becomes more appropriate as the shock layer grows. Figure 29 shows the variation of shock layer Knudsen number, defined as

$$Kn = \left[\int_{y_{INNER}}^{y_{OUTER}} \frac{dy}{\lambda} \right]^{-1},$$

with radial distance of the dividing streamline. The flow clearly is becoming less rarefied as the shock layer incorporates more mass from the jet and atmosphere.

The evolution of the density profiles from having a strong peak on the jet side to a flatter disk-like shape with a defect near the jet shock is evident in these figures. These factors affect this behavior: first, the temperature behind the air shock decreases; second, the density of the undisturbed flow upstream of the shock decreases; third, a fairly high pressure difference across the shock layer is needed to turn the flow in the downstream parts of the shock layer toward the axis because of its greater mass flow. At x_{DSL} = 10 km (Figure 27), the jet shock is probably becoming rather thick in relation to the gradient scale of the adjacent internal flow.

The composition profiles are, for the most part, unremarkable. We see that in the upstream parts of the shock layer all species diffuse rapidly. In the downstream regions, the H_2 profiles tend to be flatter and the exhausterator hydrocarbon

("HC") profiles to be steeper than those of the other exhaust species mobility. Little separation of atomic oxygen from the atmospheric species is evident except at the inner edge of the shock layer where concentrations are very low.

Scaling: The application of these computations to the flow from an engine of different size can be ascertained by examining the scaling laws[10] that govern the interaction region. The flow field in the shock layer is viscous, and thus in addition to the inviscid scaling parameters $\sqrt{F/P_\infty L^2}$ and M_∞ which describe the gross aspects of the structure one must keep temperature and plume Knudsen number constant. Of course, plume and atmospheric composition must also remain fixed and the undisturbed plume structure must scale geometrically if detailed results are to be identical in the two different flows. The latter requirement is essentially that the engine be scaled, and that the scale not be so small that viscous effects (e.g., wall boundary layer formation) occupy more than a very small region of the flow. If T is constant, then

$$Kn \sim \frac{1}{P_\infty L}$$

and combination of this with the gross scaling law yields

$$Kn \sim \sqrt{FP_\infty} \quad .$$

The scaling of these results to an engine of different thrust is thus done as follows: let the vehicle be at a different thrust and ambient pressure such that FP_∞ is the same value as that of these calculations. Keep the same ambient temperature and composition and the same geometrical structure

and relative total temperature and composition distribution as in this undisturbed flow field, but scaled according to $L \sim \sqrt{F}$. Then the shock layer flow will scale as

$$L \sim F$$

or in words, the size of the shock layer will be proportional to the vehicle thrust if its internal structure is to be identical. It is important to recognize that in a flow with significant viscous effects, one cannot choose both F and P_∞ arbitrarily if the temperature and composition distributions are to map into the scaled flow.

FUTURE WORK

Our immediate plans are to carry this flow field further downstream toward the region of pressure equilibration. These computations are now in progress. The altitude chosen, 140 km, is at (or a little beyond) the upper limit of validity of our results in the bow region, as we expected from preliminary considerations. It would be desirable to have calculations at low altitudes; these would allow the altitude dependence of the plume chemistry to be determined. Although the bow region calculation should become progressively less realistic at higher altitudes, the downstream portion of the plume should continue to be reasonably well described for at least another order of magnitude change in ambient density. It may therefore be reasonable to attempt a calculation at a somewhat higher altitude.

Modifications to the computational procedures will be necessary to allow the entire plume to be well described at a higher altitude. The most obvious modification would be allowing the shock waves to become thick, and to extend the calculations into the fully merged flow regime, while continuing to employ a continuum treatment. It is not clear that this approach will be fruitful. A recent analysis[14] of the merged-layer regime for blunt-body flows (at λ_∞/R_n = 0.1 and 0.02), using a Monte Carlo simulation procedure for solving the Boltzmann equation, indicates that rather significant differences exist between these solutions and those obtained using the thin-layer approximation to the Navier-Stokes equations. How much of this discrepancy is due to the difference between continuum and molecular descriptions and how much to the thin-layer approximation is not clear. However,

the Monte Carlo results do indicate that in the outer portions of the flow, where formation of the shock dominates, the velocity distribution is non-Maxwellian. Deviations from translational equilibrium in the region of mixing between the exhaust and the atmosphere will affect the shock layer chemistry, particularly when the activation energy of a process is greater than about 10 k cal/mole. We believe that this behavior makes it more reasonable to proceed directly to a solution of the Boltzmann equation than to attempt a thick-shock continuum calculation. We are currently investigating the application of Monte Carlo and other procedures to the exhaust flow field.

References

1. F. P. Boynton, "The MULTITUBE Supersonic Flow Computer Code," General Dynamics/Convair Report GDC-DBE67-003, February 1967.

2. R. F. Probstein and N. H. Kemp, J. Aerospace Sci. 27, 174 (1960)

3. F. P. Boynton and A. Thomson, J. Computational Phys. 3, 379 (1969)

4. S. Fenster and E. Miller (Aerospace Corporation, San Bernardino, California), private communications

5. J. Bowyer, L. D'Attore, and H. Yoshihara, "Transonic Aspects of Hypervelocity Rocket Plumes," Supersonic Flow, Chemical Processes, and Radiative Transfer, ed. by. D. B. Olfe and V. Zakhay (Pergamon Press, London, 1964), pp. 201-210

6. D. W. Eastman and L. P. Radtke, AIAA J. 1, 918 (1963)

7. T. C. Adamson and J. A. Nicholls, J. Aeronaut. Sci. 26, 16 (1959)

8. M. Abbett, "The Mach Disc in Underexpanded Exhaust Plumes," AIAA Paper 70-231

9. L. D'Attore and F. Harshbarger, "Experimental and Theoretical Studies of Underexpanded Jets Near the Mach Disc," General Dynamics/Astronautics Report GDA-DBE64-008, February 1964

10. A. Thomson, "High-Altitude Rocket Plume Structure," General Dynamics/Convair Report GDC-DBE65-023, September 1965

11. H. K. Cheng, "The Blunt-Body Problem in Hypersonic Flow at Low Reynolds Number," Cornell Aeronautical Laboratory Report No. AF-128-A-10, June 1963

12. N. W. Rosenberg

13. "COSPAR International Reference Atmosphere 1965," Committee on Space and Atmospheric Research

14. F. W. Vogenitz and G. V. Takata, "Monte Carlo Study of Blunt Body Hypersonic Viscous Shock Layers," Seventh International Rarefied Gas Dynamics Symposium (1970)

Nomenclature

A	Streamtube area
c_i	Species mass fraction
D_{ij}	Binary diffusion coefficient
D_i^T	Thermal diffusion coefficient
F	Vehicle thrust
$\overline{F}_{10,7}$	Solar flux at 10.7 cm
H	Total enthalpy
h_i	Specific enthalpy
$\overline{h}_i$	Partial molar enthalpy
J_i	Species mass flux
K	Streamline curvature
L	Characteristic length
M	Mach number
Kn	Knudsen number
$\dot{m}$	Mass flow rate
P	Pressure
q	Heat flux
Pr	Prandtl number
R_n	Nose radius
Re	Reynolds number
r	Radial distance from axis
S	Entropy

s	Distance in streamwise direction
T	Temperature
u	Flow speed
Sc	Schmidt number
x	Axial distance
x_i	Species mole fraction
y	Distance normal to streamlines
φ	Flow angle (with respect to axis)
λ	Mean free path
ρ	Density

Subscripts

k	Streamline and streamtube index
ℓ	Index of surface normal to streamlines
i	Species index
∞	Ambient conditions
DSL	Dividing streamline

MIXTURE RATIO, $\dot{m}_{O_2}/\dot{m}_{RP-1}$
2.5
2.0
1.5
0
0.25
0.50
0.75
1.00
RADIUS/EXHAUST RADIUS (r/r_e)

Fig. 1

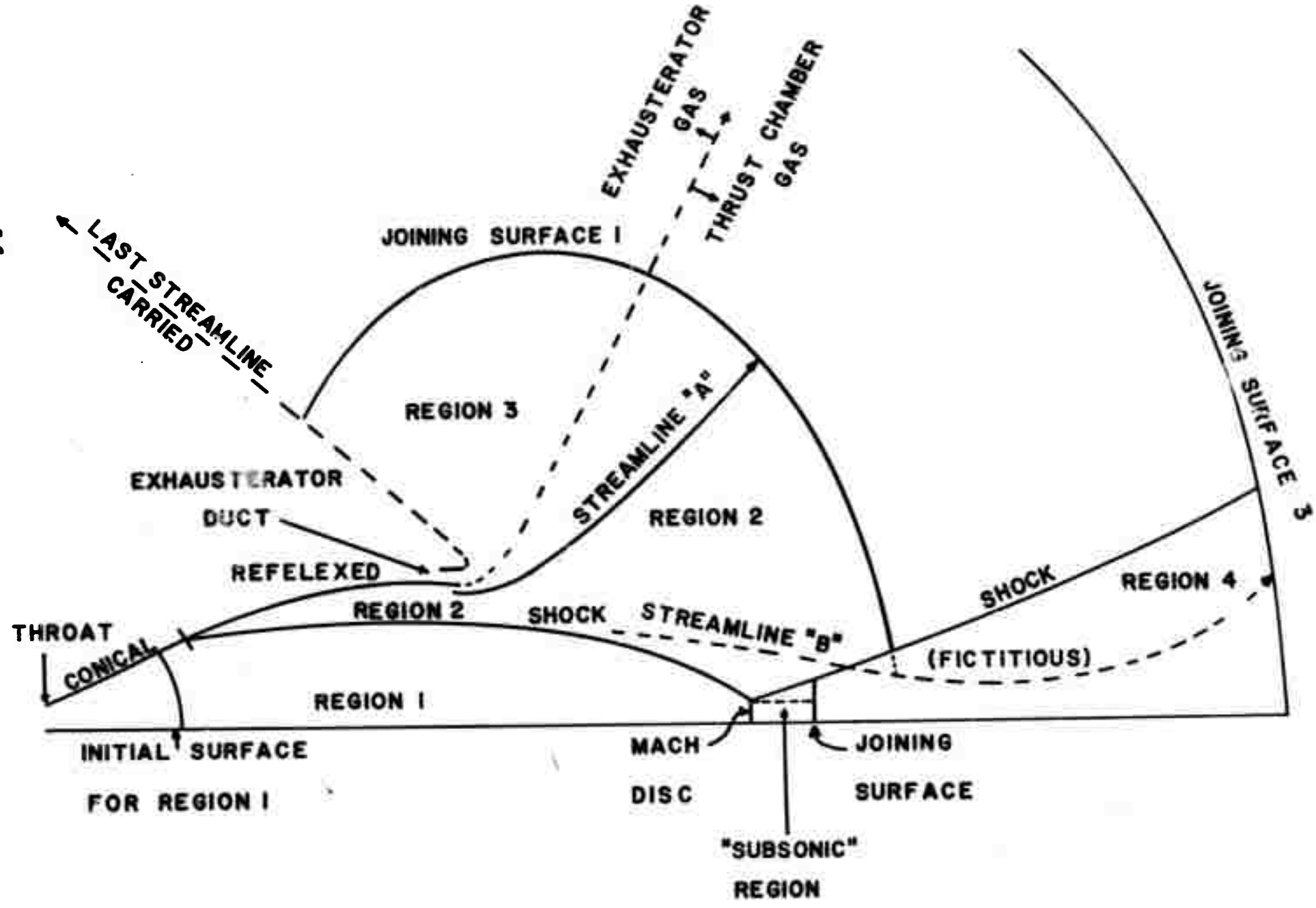
EXHAUSTERATOR GAS
THRUST CHAMBER GAS
LAST STREAMLINE CARRIED
JOINING SURFACE 1
JOINING SURFACE 3
REGION 3
STREAMLINE "A"
EXHAUSTERATOR DUCT
REGION 2
REFELEXED
SHOCK
REGION 4
REGION 2
SHOCK
STREAMLINE "B"
THROAT
CONICAL
(FICTITIOUS)
REGION 1
INITIAL SURFACE FOR REGION 1
MACH DISC
JOINING SURFACE
"SUBSONIC" REGION

Fig. 2

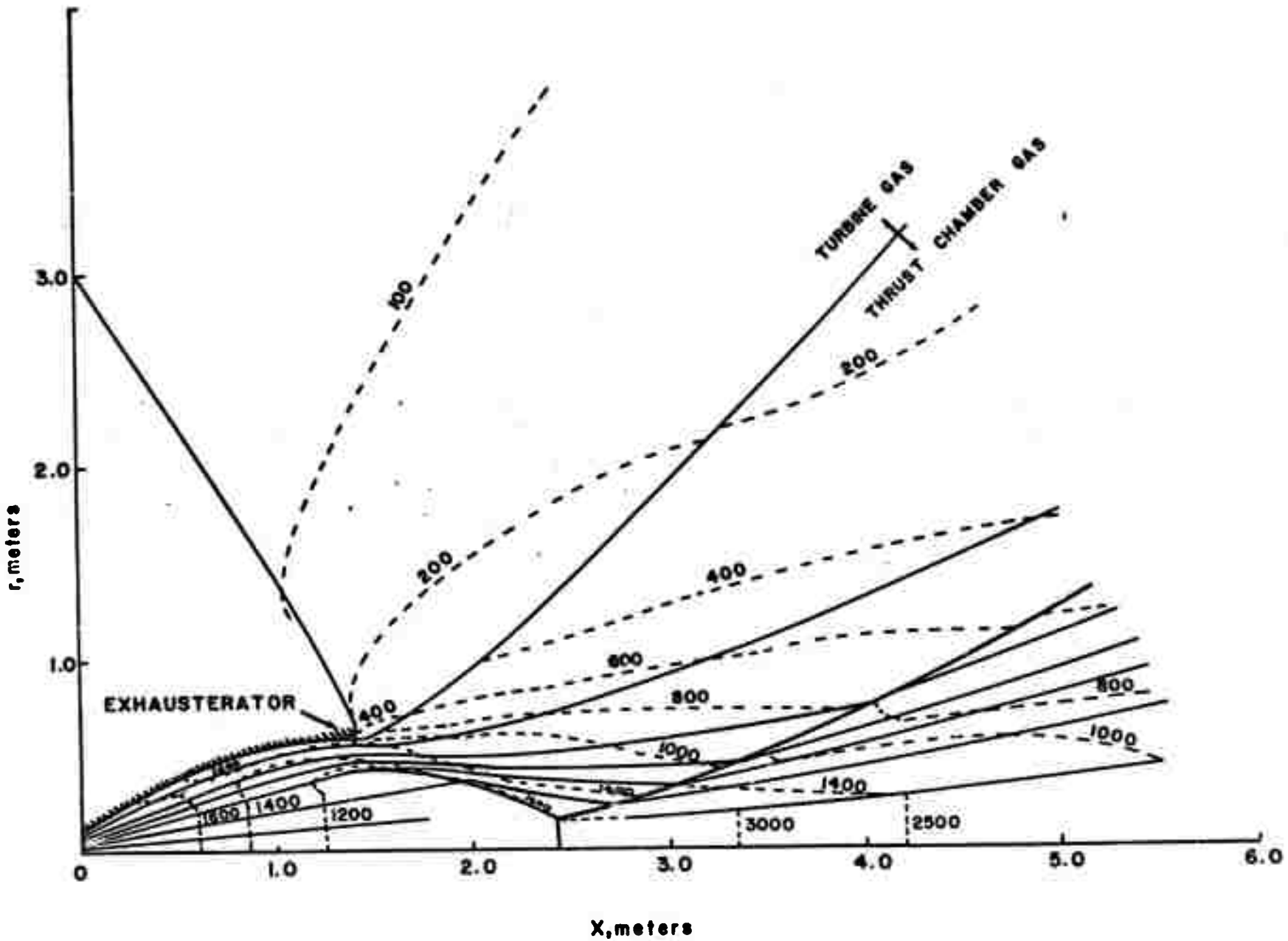
TURBINE GAS
THRUST CHAMBER GAS
100
200
400
600
800
1000
1400
EXHAUSTERATOR
1600
1400
1200
3000
2500
3.0
2.0
1.0
0
1.0
2.0
3.0
4.0
5.0
6.0
r, meters
X, meters

Fig. 3

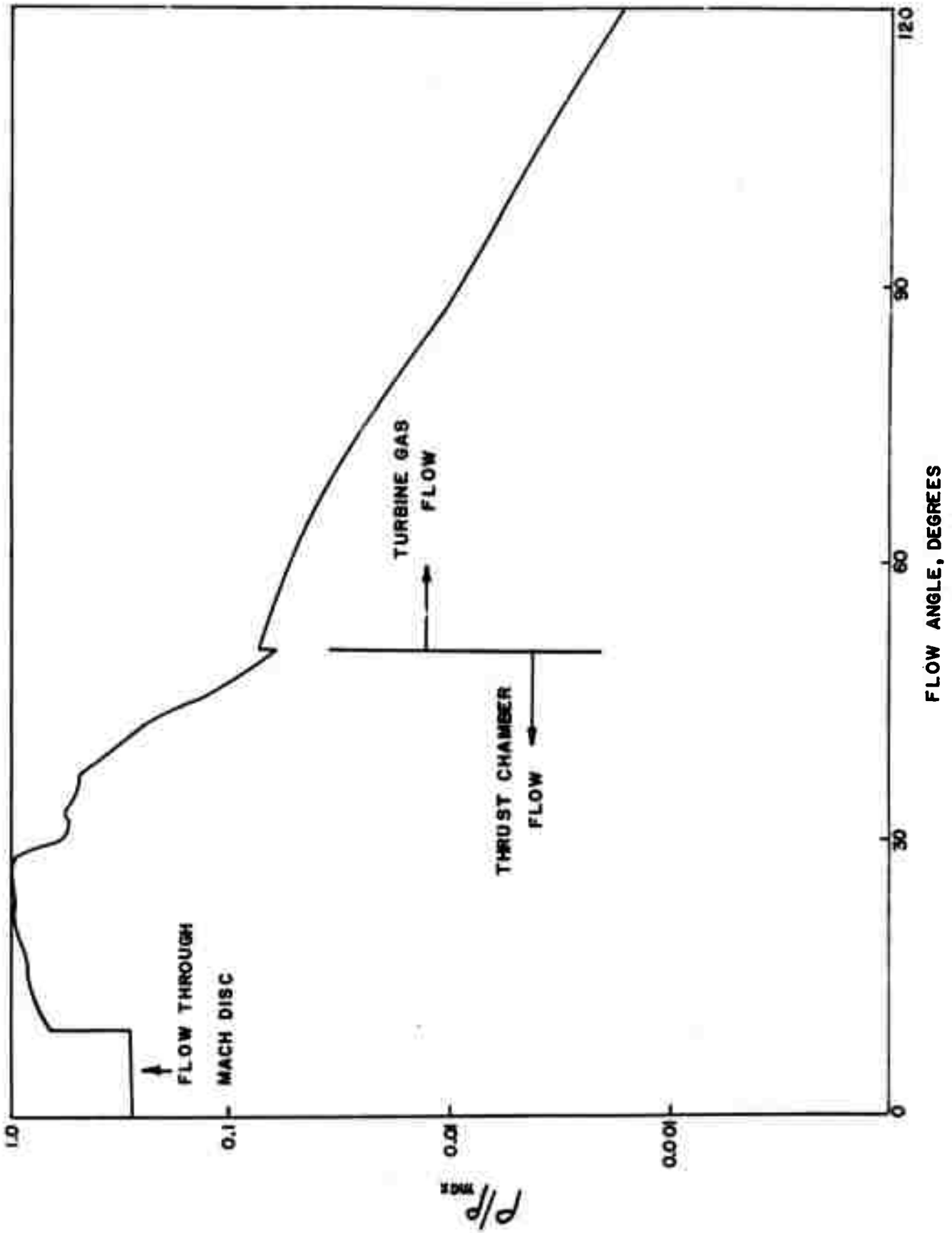
1.0
0.1
0.01
0.001
P/P_{MAX}
0
30
60
90
120
FLOW ANGLE, DEGREES
FLOW THROUGH
MACH DISC
THRUST CHAMBER
FLOW
TURBINE GAS
FLOW

Fig. 4

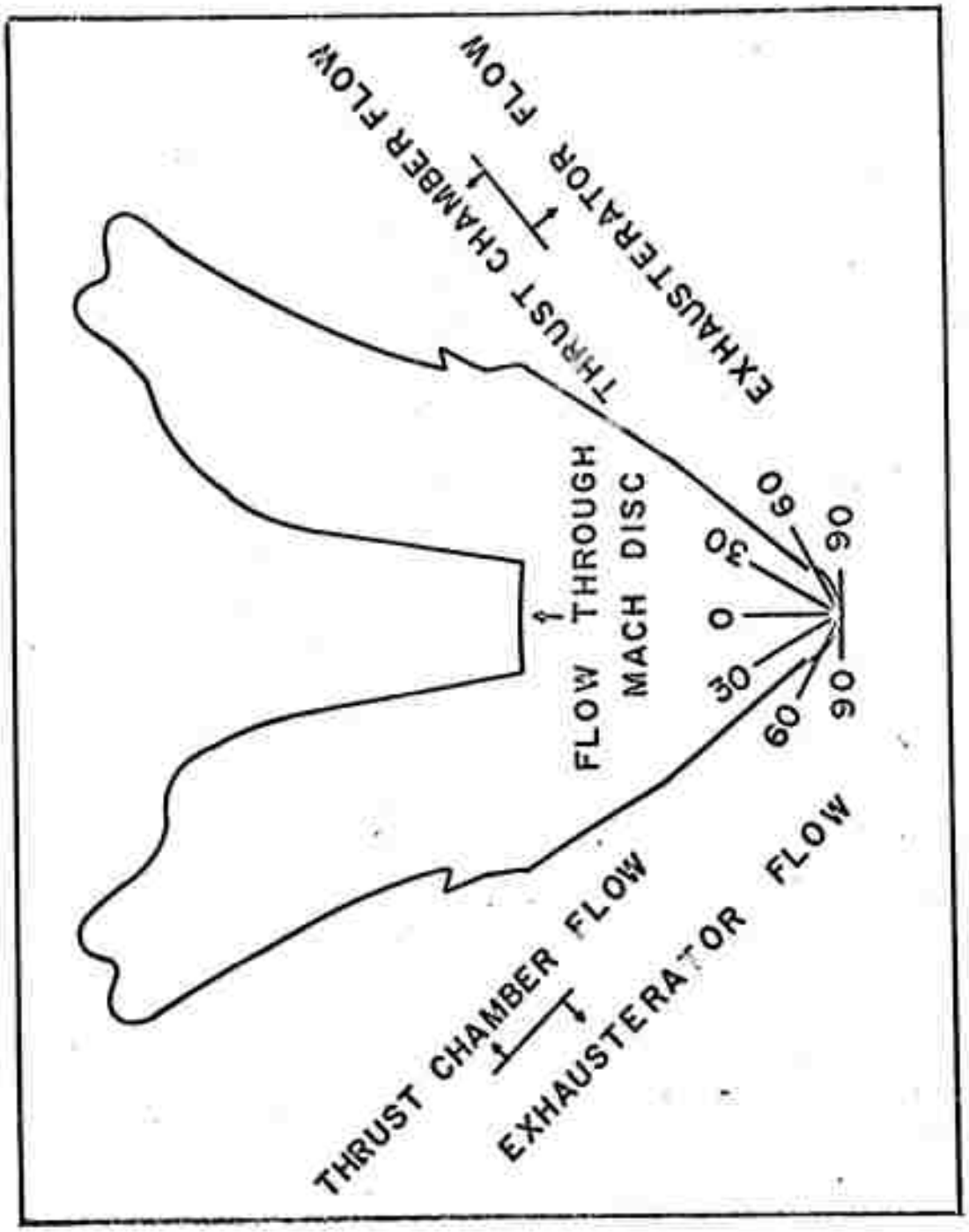
EXHAUSTERATOR FLOW
THRUST CHAMBER FLOW
FLOW THROUGH MACH DISC
90
60
30
0
30
60
90
THRUST CHAMBER FLOW
EXHAUSTERATOR FLOW

Fig. 5

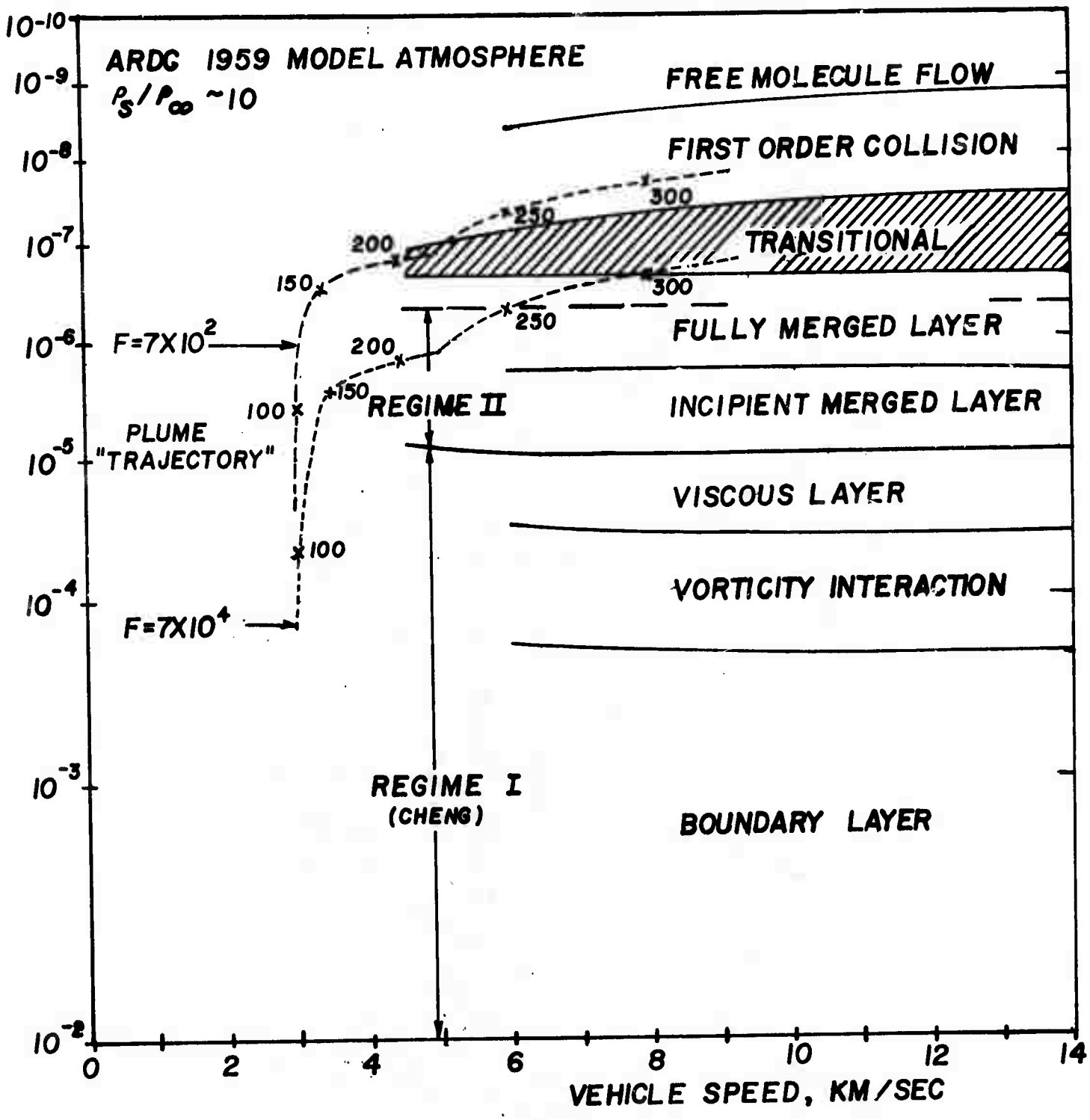

PLUME "TRAJECTORY" IN RELATION TO THE LOW DENSITY · VISCOUS REGIMES AS DEFINED BY PROBSTEIN AND BY CHENG

Fig. 6

THIRD STREAMLINE
LOCUS $\beta = \beta_c$
SECOND STREAMLINE
INITIAL PRANDTL-MEYER LINE
COMPUTED LIMITING STREAMLINE
LIMITING LINE (SONIC EXIT FLOW)

Fig. 7

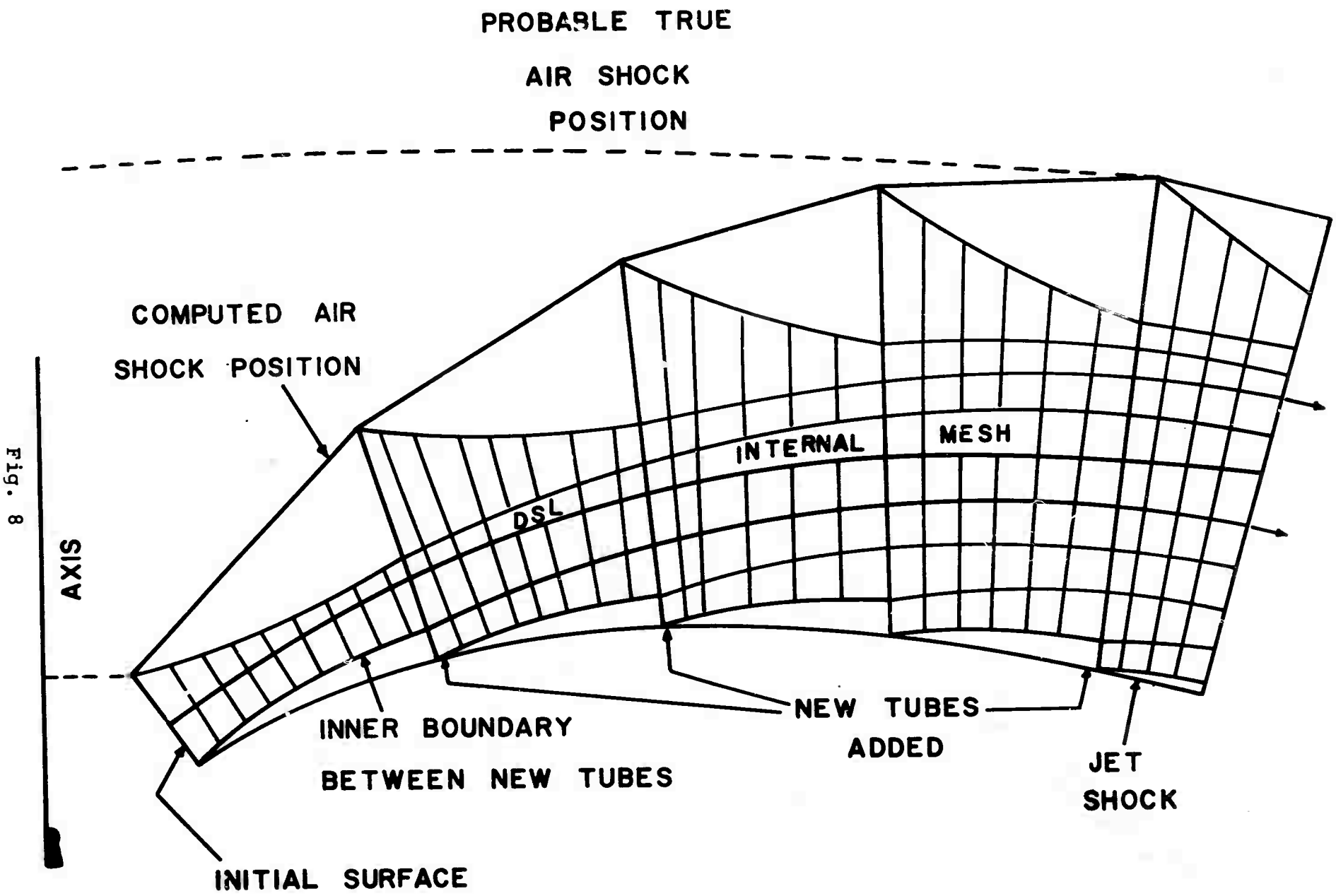
PROBABLE TRUE
AIR SHOCK
POSITION
COMPUTED AIR
SHOCK POSITION
INTERNAL
MESH
DSL
AXIS
INNER BOUNDARY
BETWEEN NEW TUBES
NEW TUBES
ADDED
JET
SHOCK
INITIAL SURFACE

Fig. 8

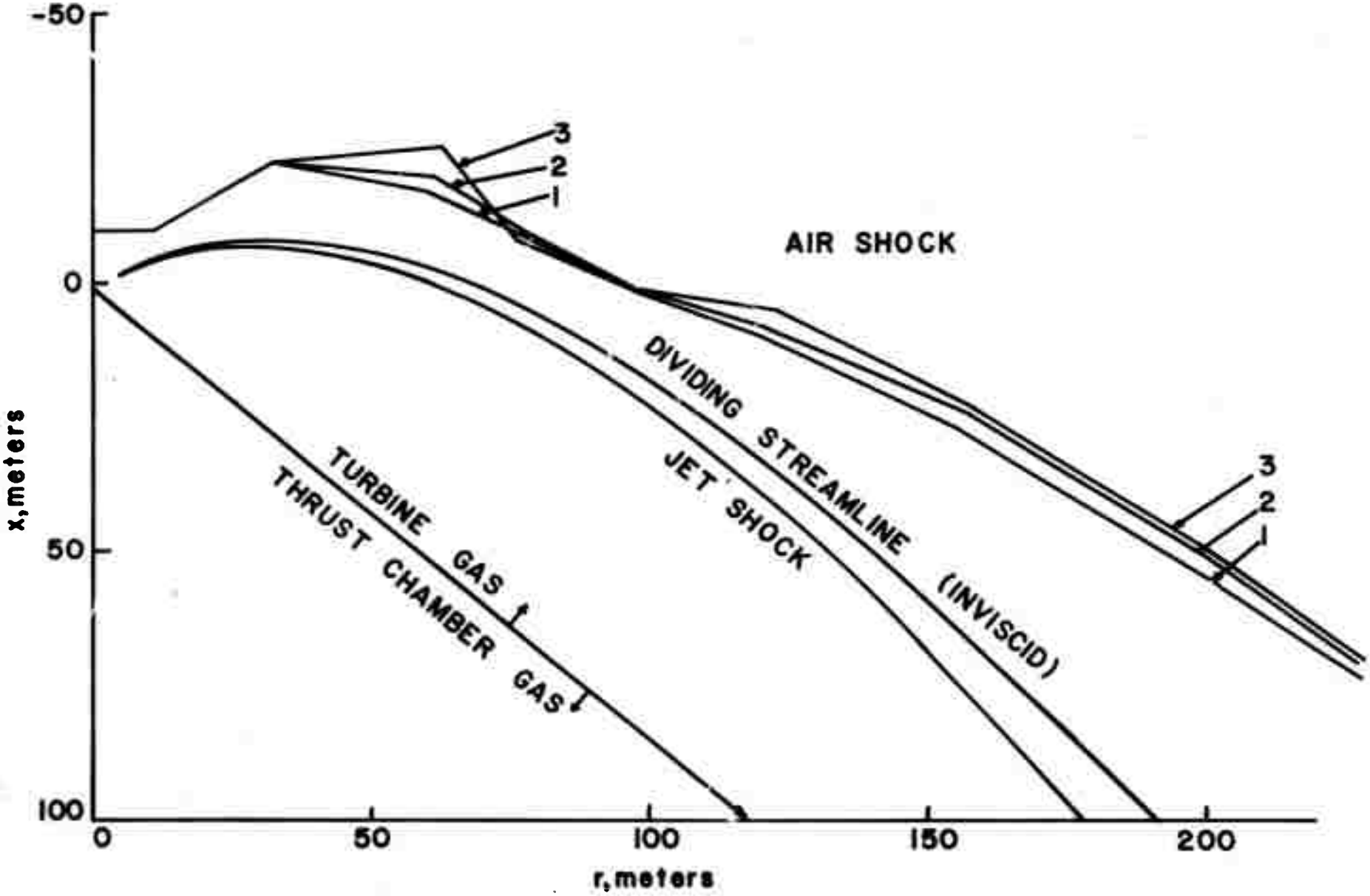
-50
0
50
100
x, meters
0
50
100
150
200
r, meters
3
2
1
AIR SHOCK
DIVIDING STREAMLINE (INVISCID)
JET SHOCK
TURBINE GAS
THRUST CHAMBER GAS
3
2
1

Fig. 9

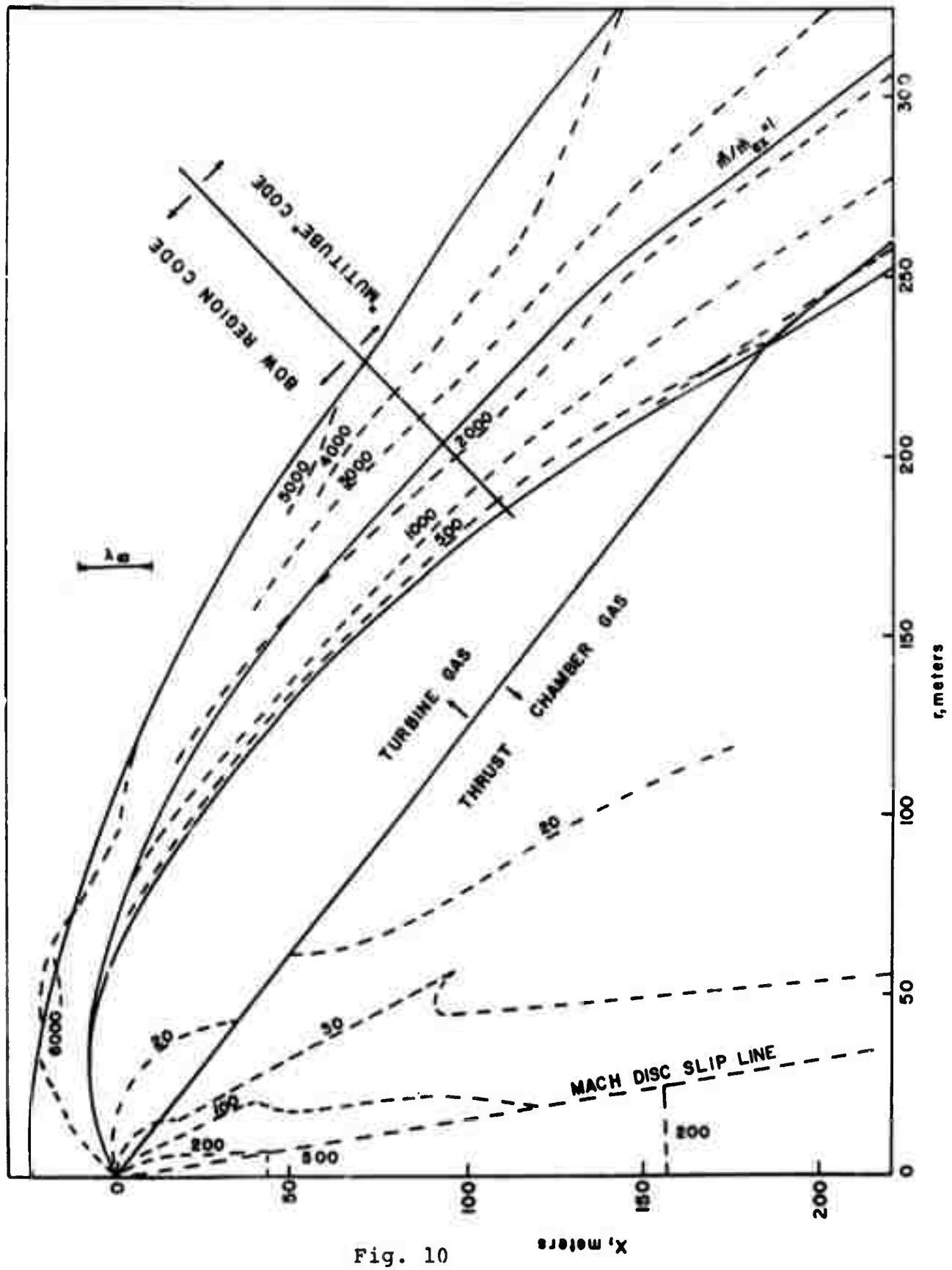
BOW REGION CODE
MULTITUBE CODE
TURBINE GAS
THRUST CHAMBER GAS
MACH DISC SLIP LINE
r, meters
X, meters

Fig. 10

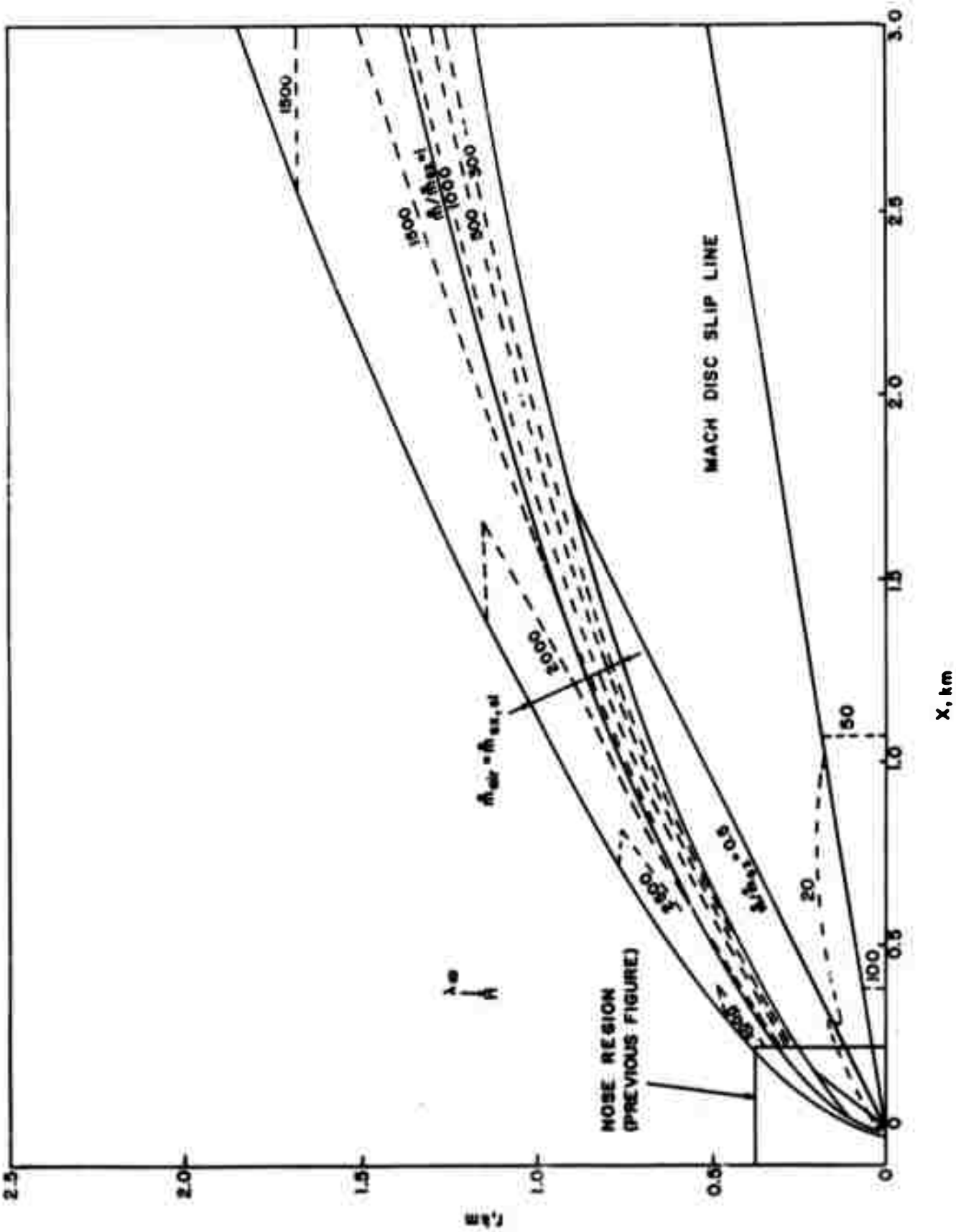
MACH DISC SLIP LINE
NOSE REGION
(PREVIOUS FIGURE)
X, km
1500
1000
500
2000
100
50
20
0
0.5
1.0
1.5
2.0
2.5
3.0

Fig. 11

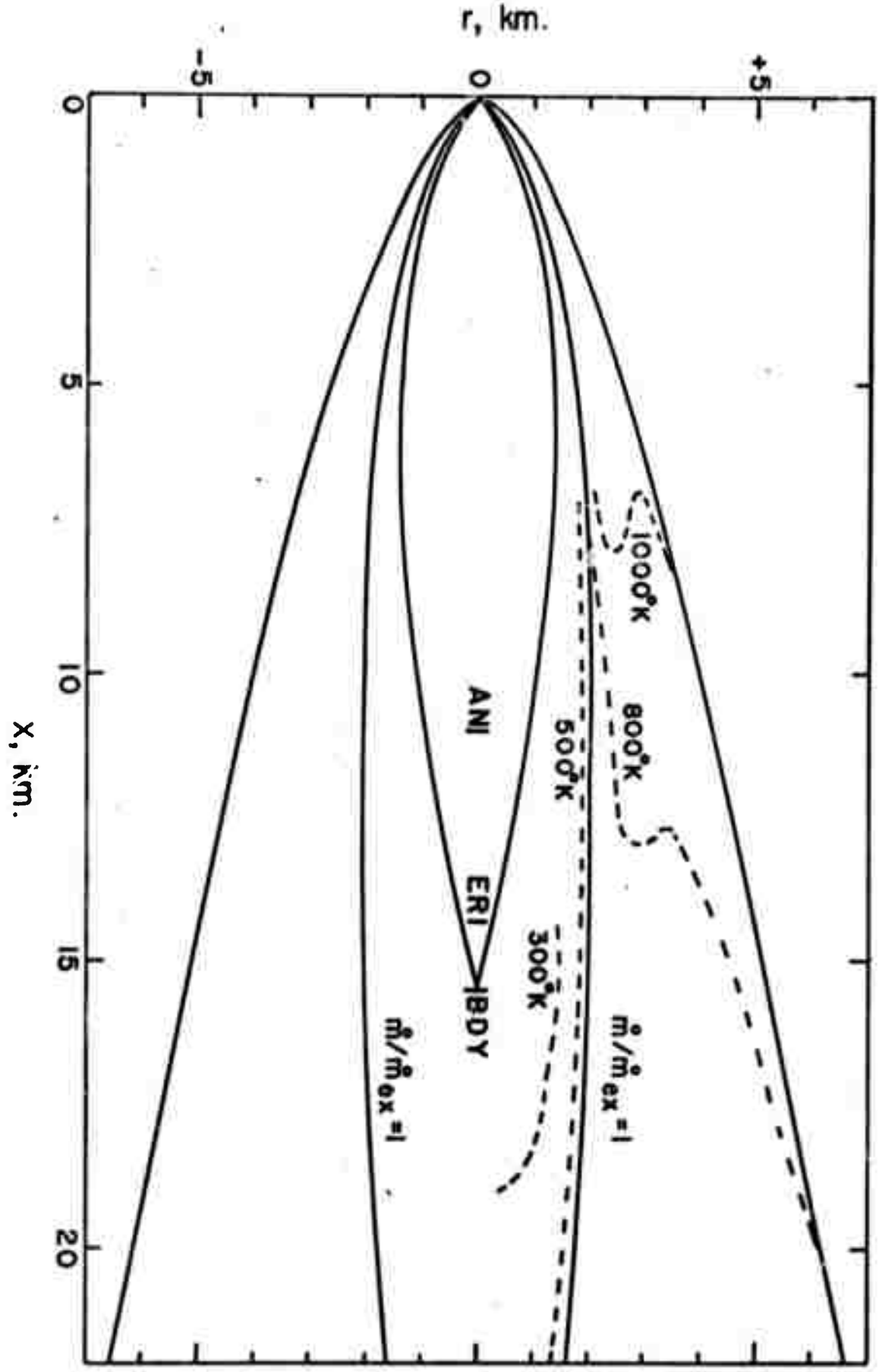
r, km.
-5
0
+5
0
5
10
15
20
x, km.
ANI
ERI
BDY
1000°K
800°K
500°K
300°K
$\dot{m}/\dot{m}_{ex}=1$
$\dot{m}/\dot{m}_{ex}=1$

Fig. 12

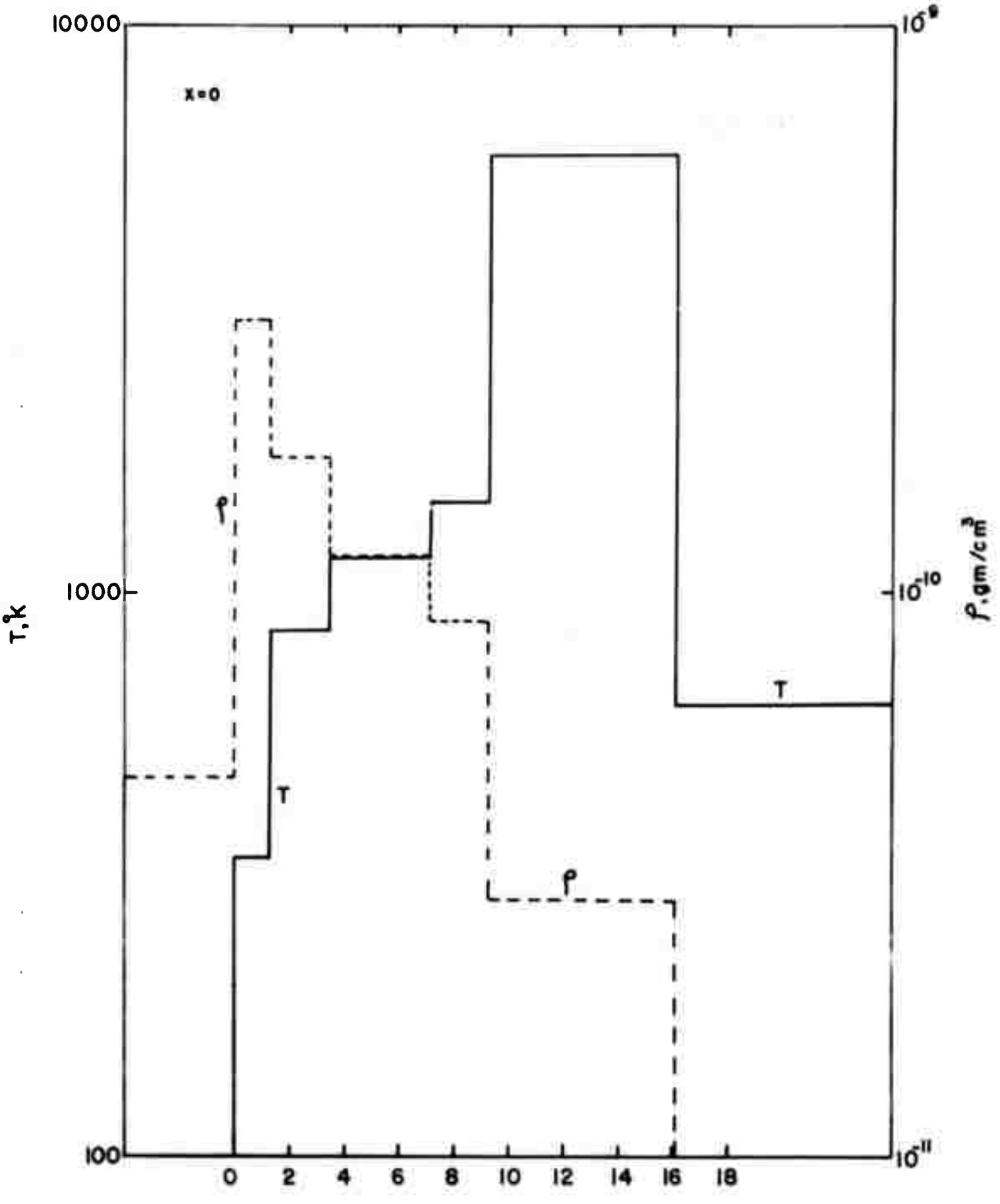
10000
1000
100
T, °K
x=0
ρ
T
T
ρ
10^{-9}
10^{-10}
10^{-11}
ρ, gm/cm³
0
2
4
6
8
10
12
14
16
18
y, meters

Fig. 13

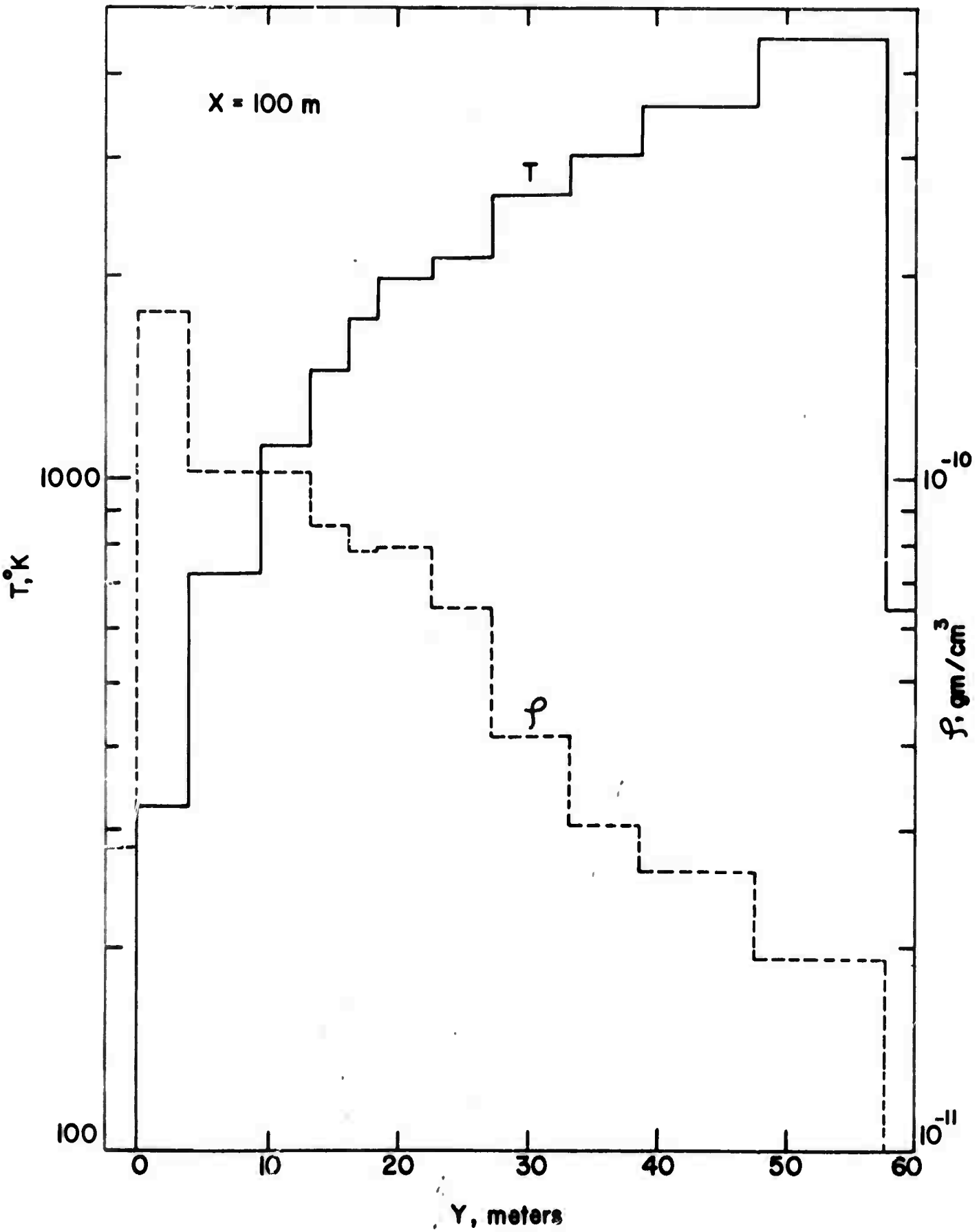
X = 100 m
T
ρ
1000
100
T, °K
10^{-10}
10^{-11}
ρ, gm/cm³
0
10
20
30
40
50
60
Y, meters

Fig. 14

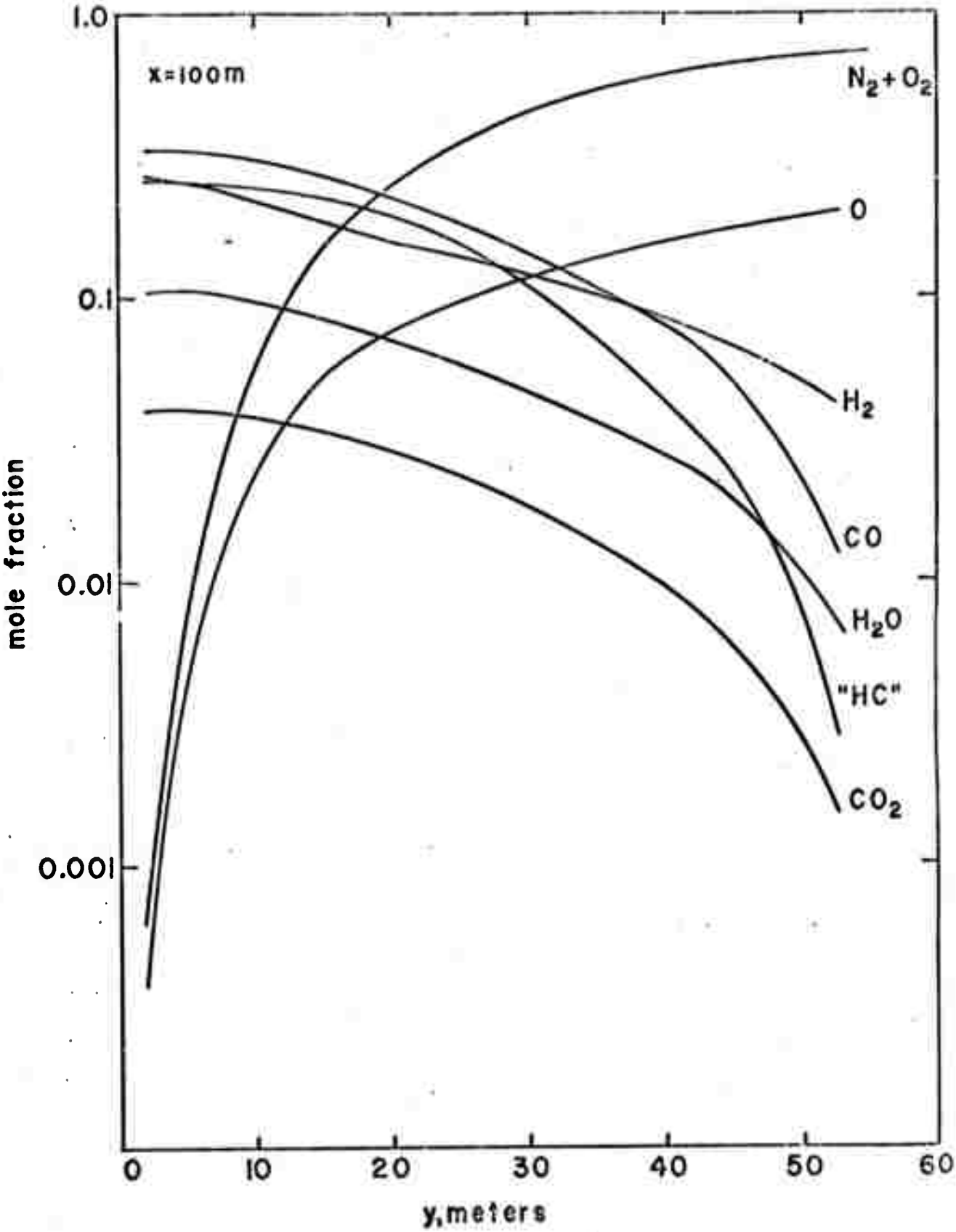
1.0
x=100m
N_2+O_2
O
0.1
H_2
CO
0.01
H_2O
"HC"
CO_2
0.001
mole fraction
0
10
20
30
40
50
60
y, meters

Fig. 15

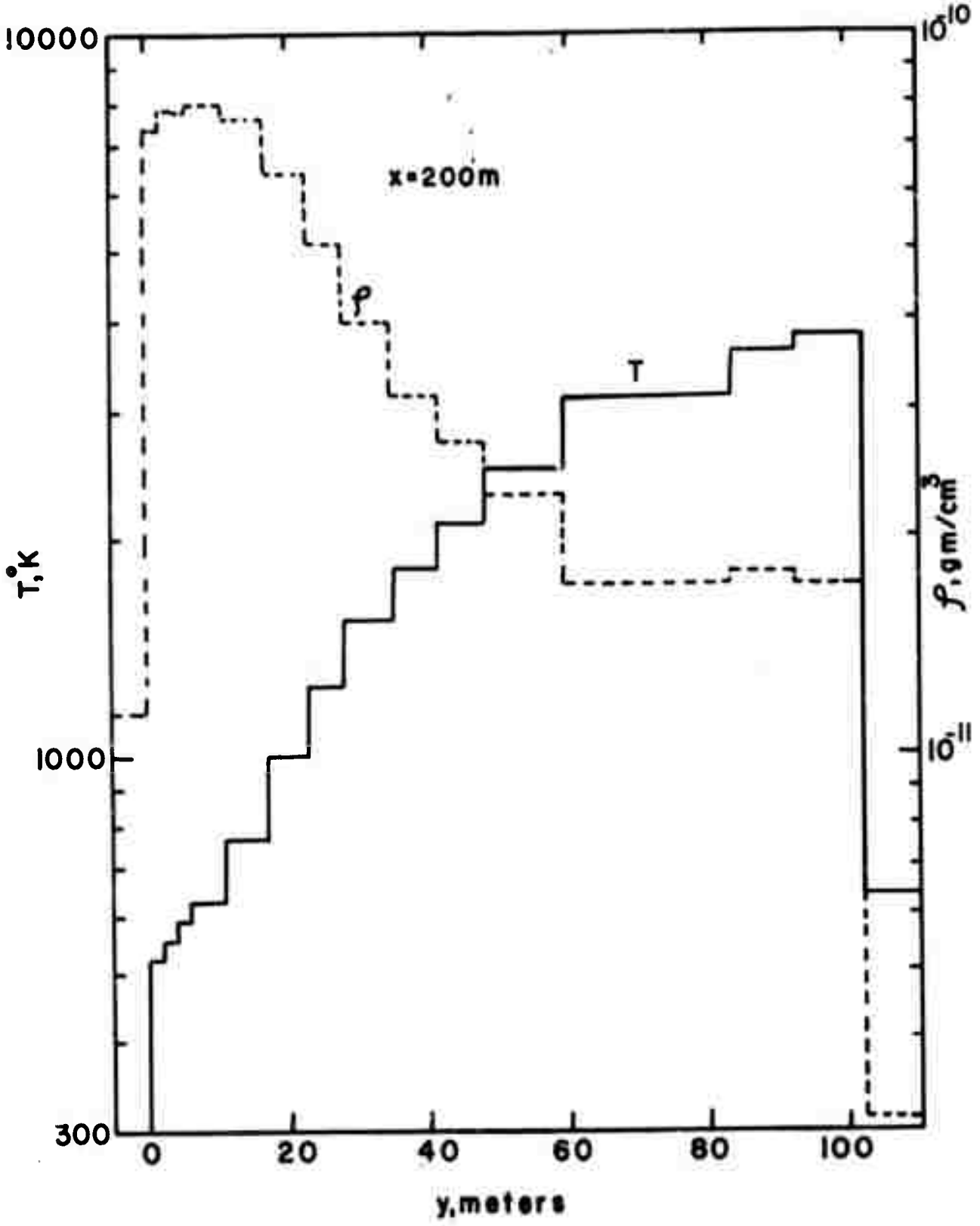
10000
1000
300
10^{10}
10^{11}
x=200m
ρ
T
T,°K
ρ, gm/cm³
0
20
40
60
80
100
y, meters

Fig. 16

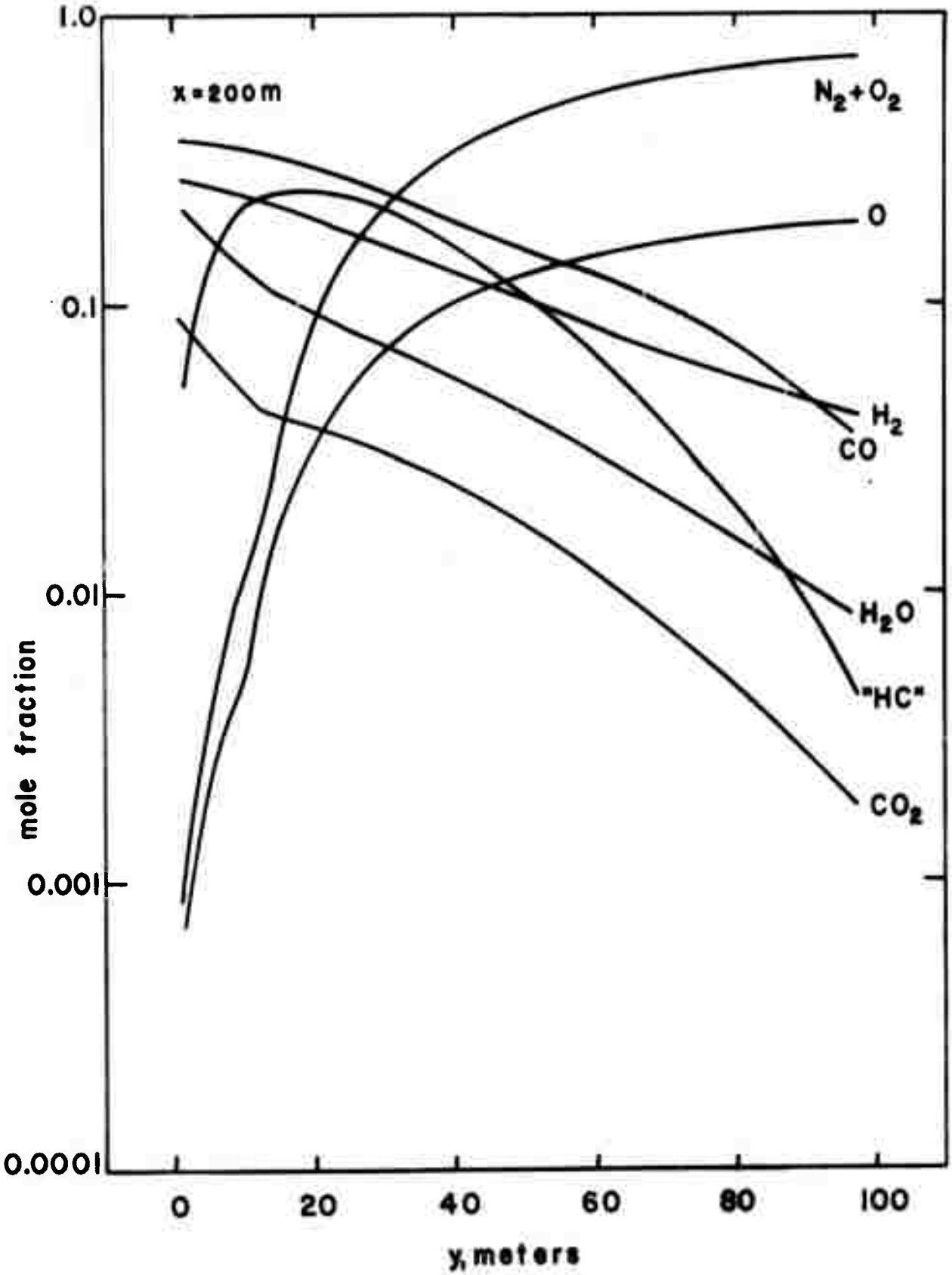
1.0
0.1
0.01
0.001
0.0001
x=200m
N_2+O_2
O
H_2
CO
H_2O
"HC"
CO_2
mole fraction
0
20
40
60
80
100
y, meters

Fig. 17

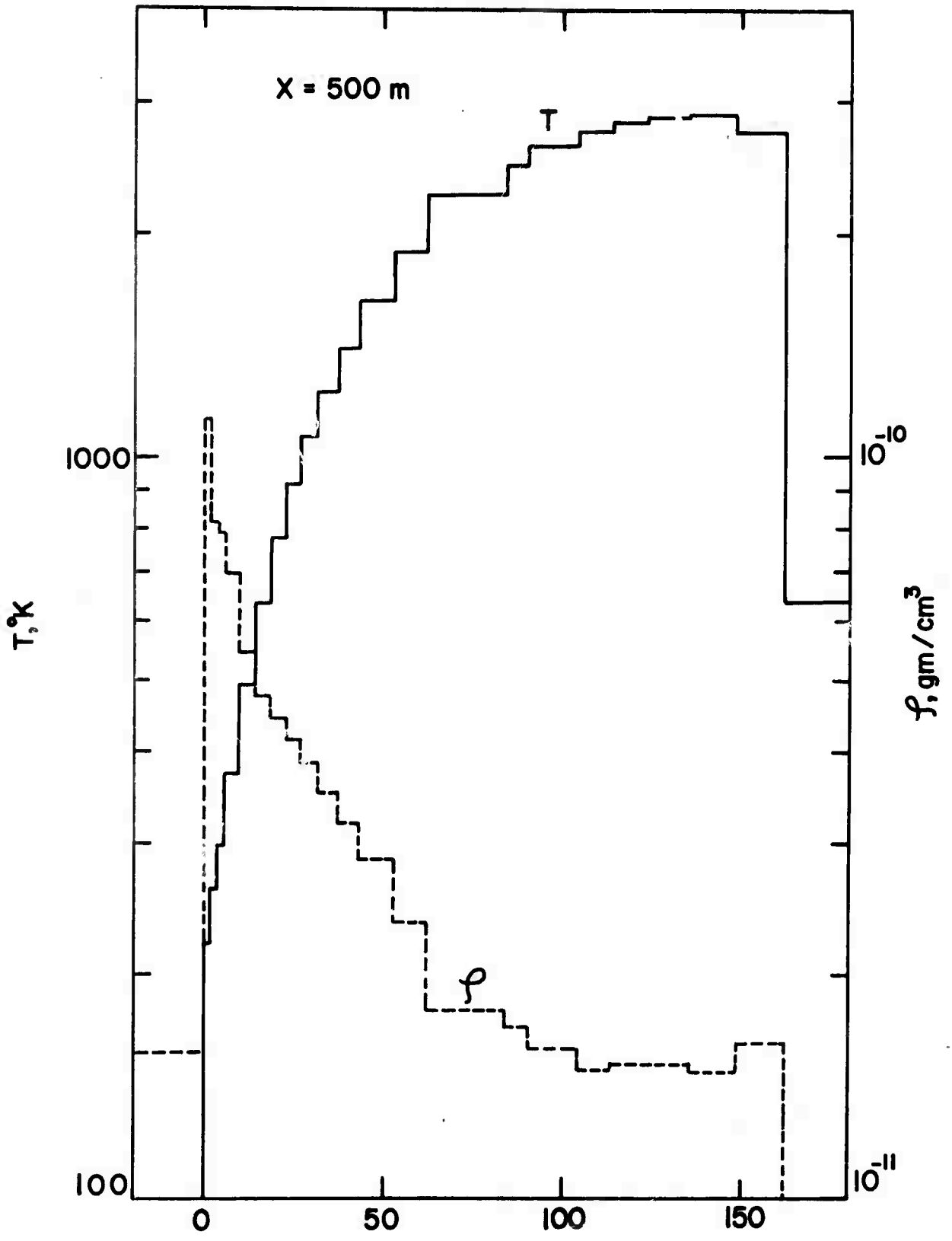

Fig. 18

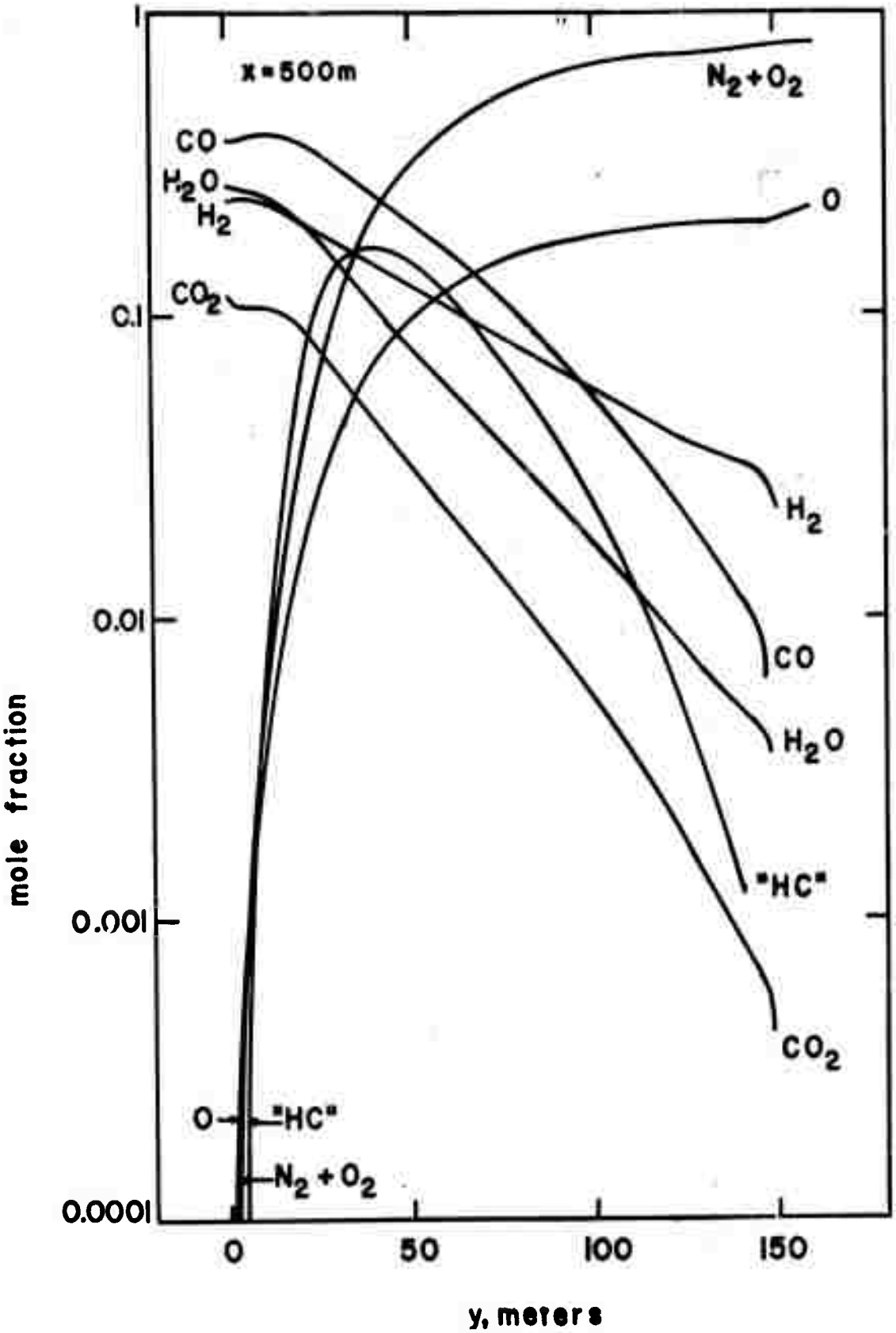
x=500m
N_2+O_2
CO
H_2O
H_2
O
CO_2
"HC"
1
0.1
0.01
0.001
0.0001
0
50
100
150
mole fraction
y, meters

Fig. 19

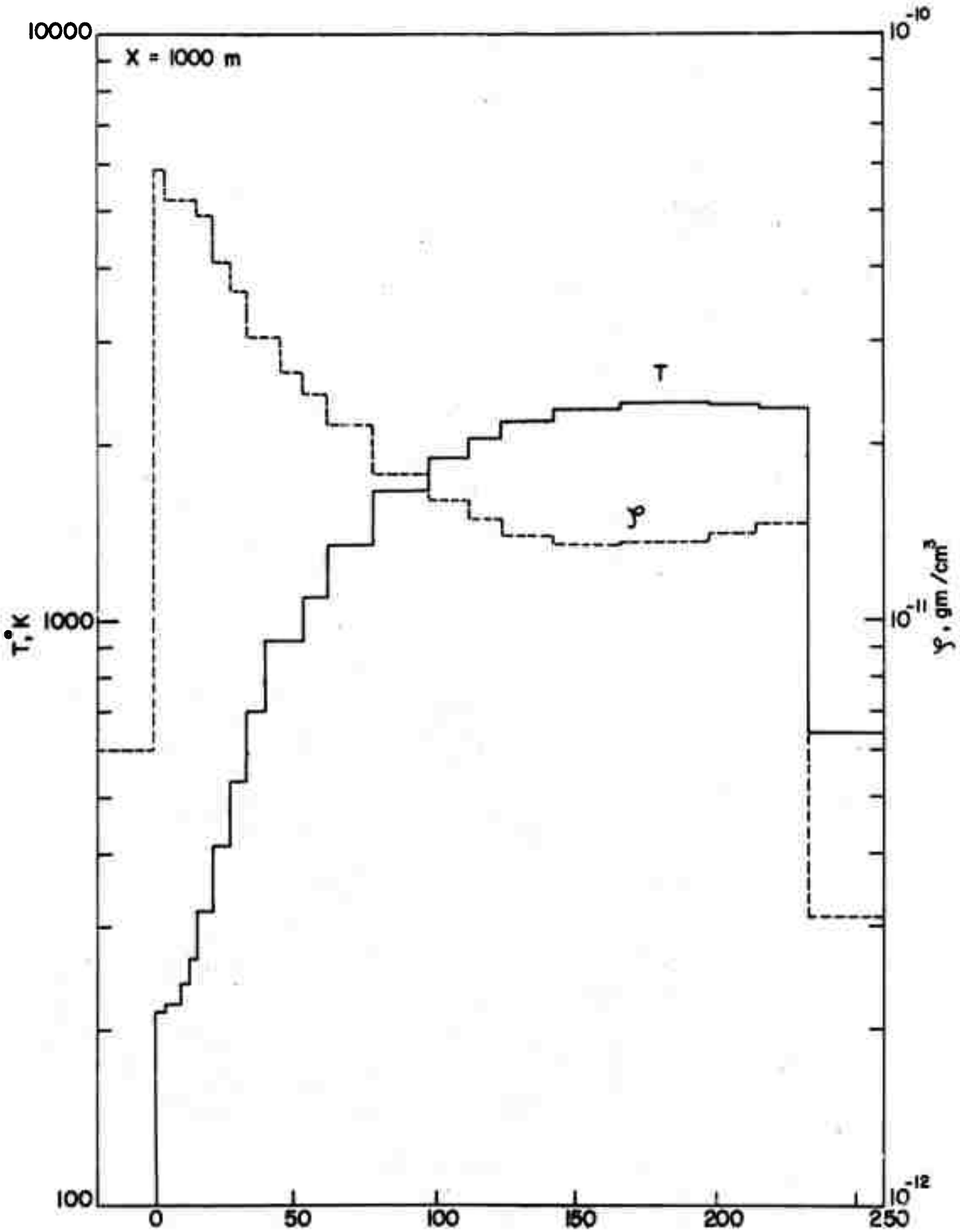
X = 1000 m
T
ρ
10000
1000
100
T, °K
10^{-10}
10^{-11}
10^{-12}
ρ, gm/cm³
0
50
100
150
200
250
Y, meters

Fig. 20

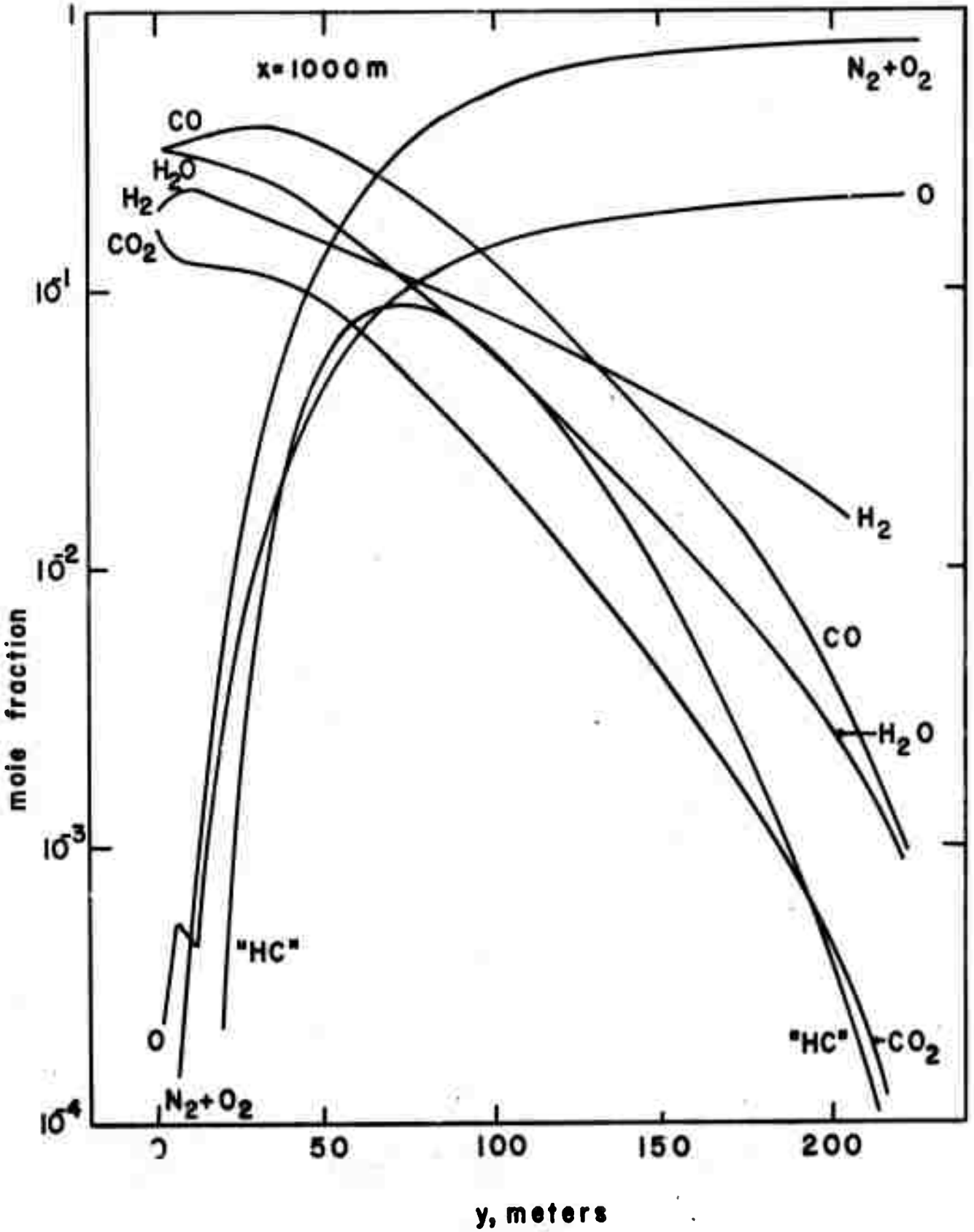
x=1000m
N_2+O_2
CO
H_2O
H_2
CO_2
O
H_2
CO
H_2O
"HC"
O
N_2+O_2
"HC"
CO_2
1
10^{-1}
10^{-2}
10^{-3}
10^{-4}
mole fraction
0
50
100
150
200
y, meters

Fig. 21

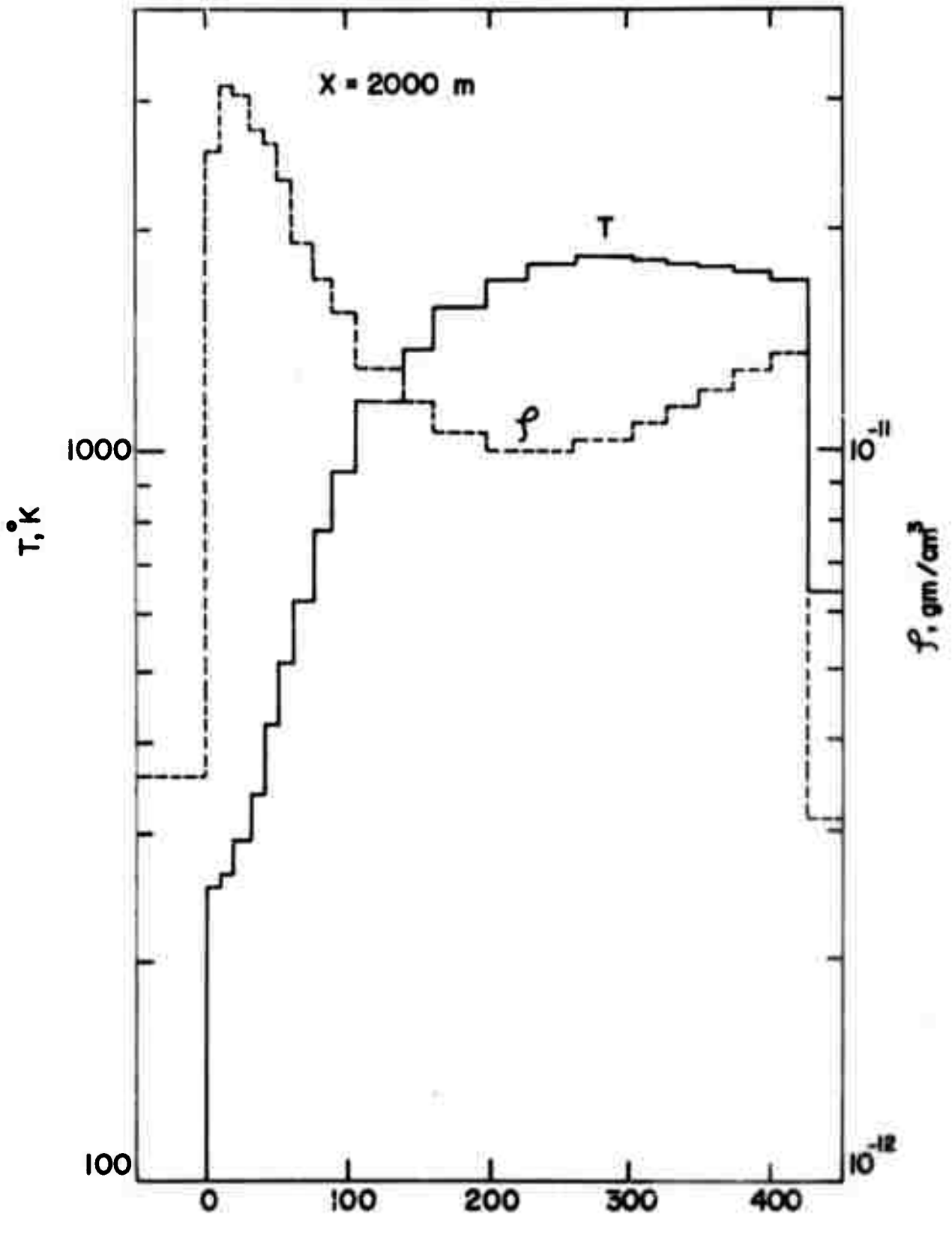
X = 2000 m
T
ρ
1000
100
10^{-11}
10^{-12}
T, °K
ρ, gm/cm³
0
100
200
300
400
Y, meters
Fig. 22

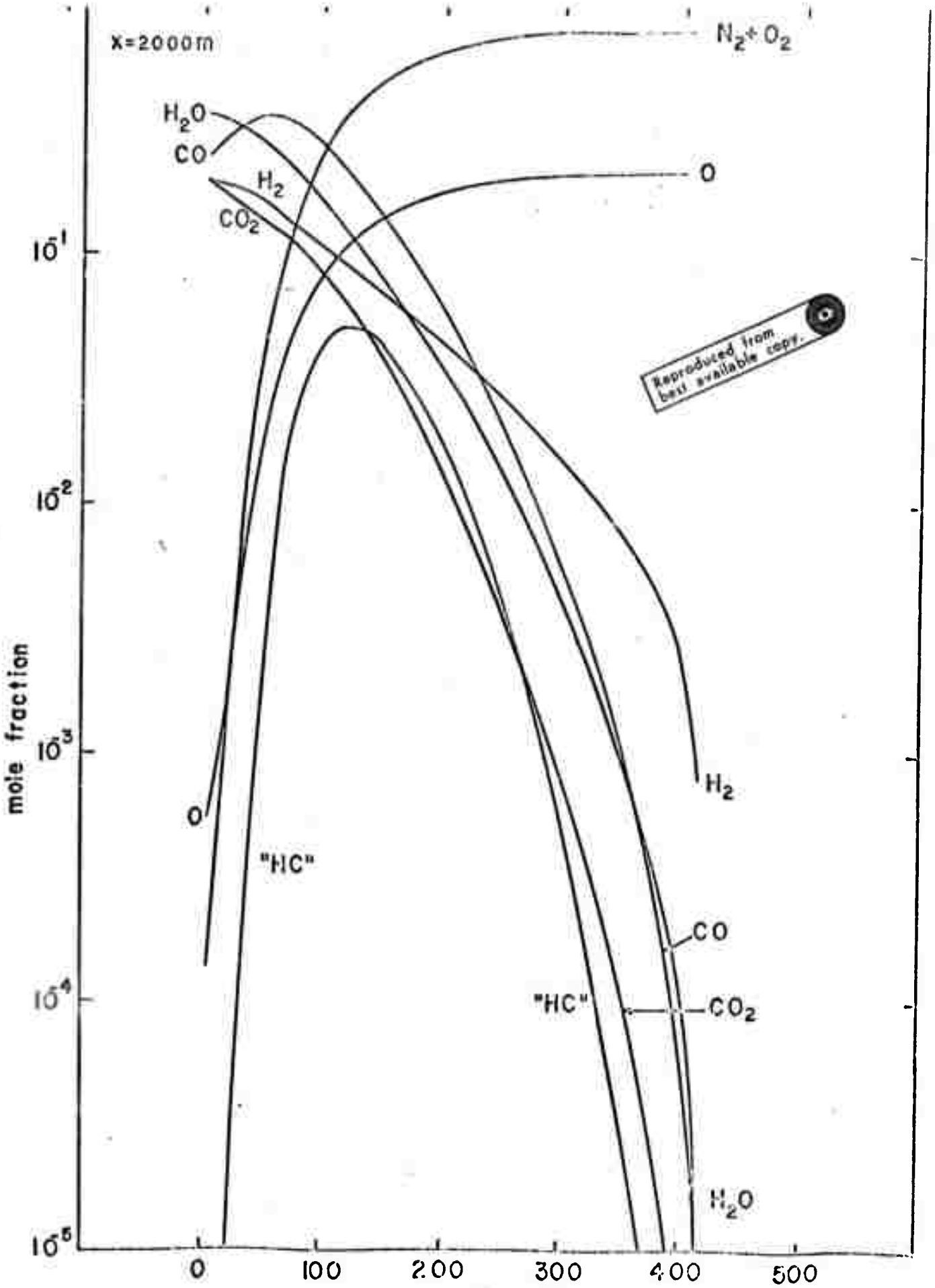
x=2000m
N_2+O_2
H_2O
CO
H_2
CO_2
O
10^{-1}
10^{-2}
10^{-3}
10^{-4}
10^{-5}
mole fraction
Reproduced from best available copy.
H_2
O
"HC"
CO
"HC"
CO_2
H_2O
0
100
200
300
400
500
y, meters

Fig. 23

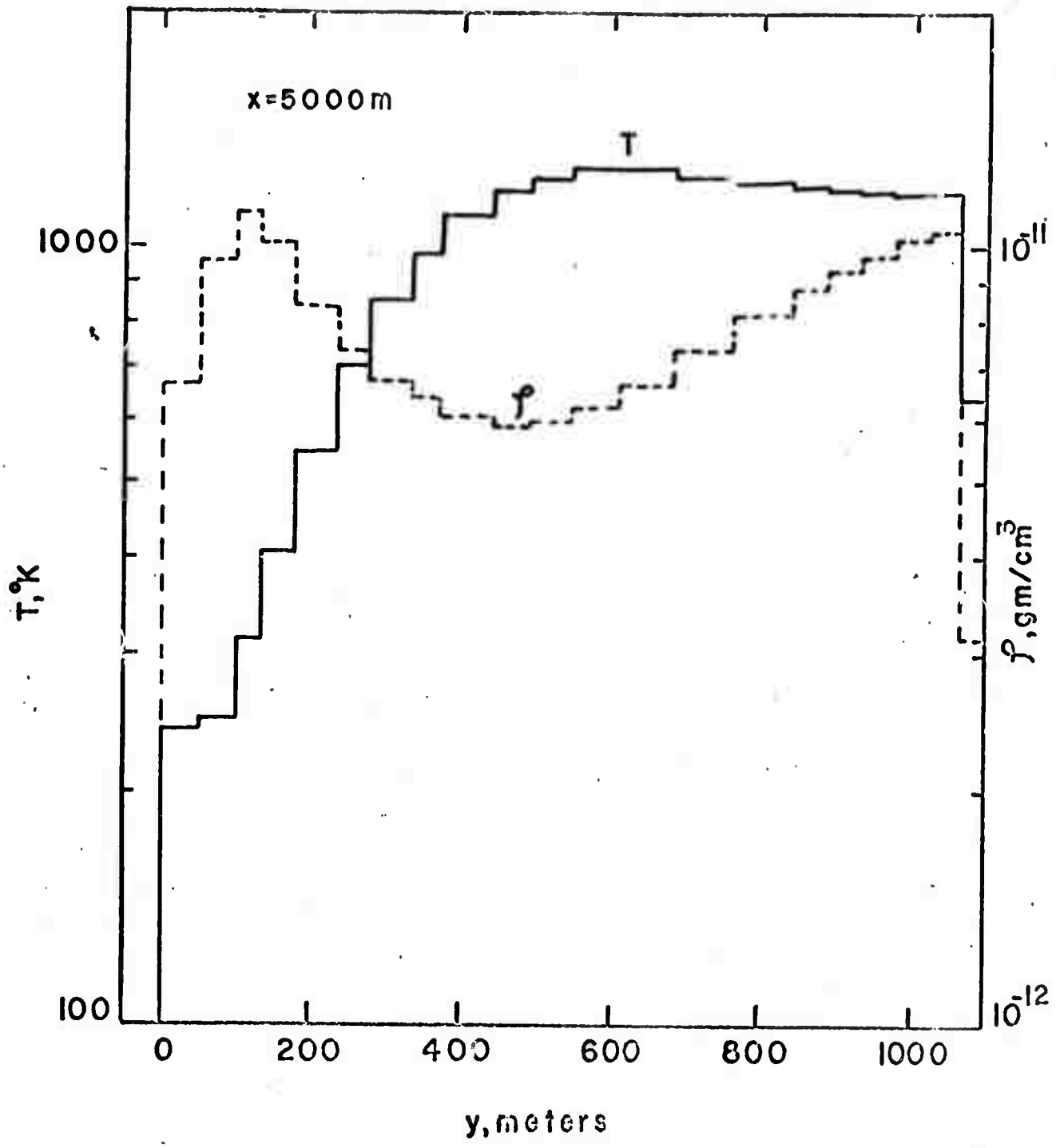
x=5000m
T
ρ
1000
100
10^{-11}
10^{-12}
T, °K
ρ, gm/cm³
0
200
400
600
800
1000
y, meters

Fig. 24

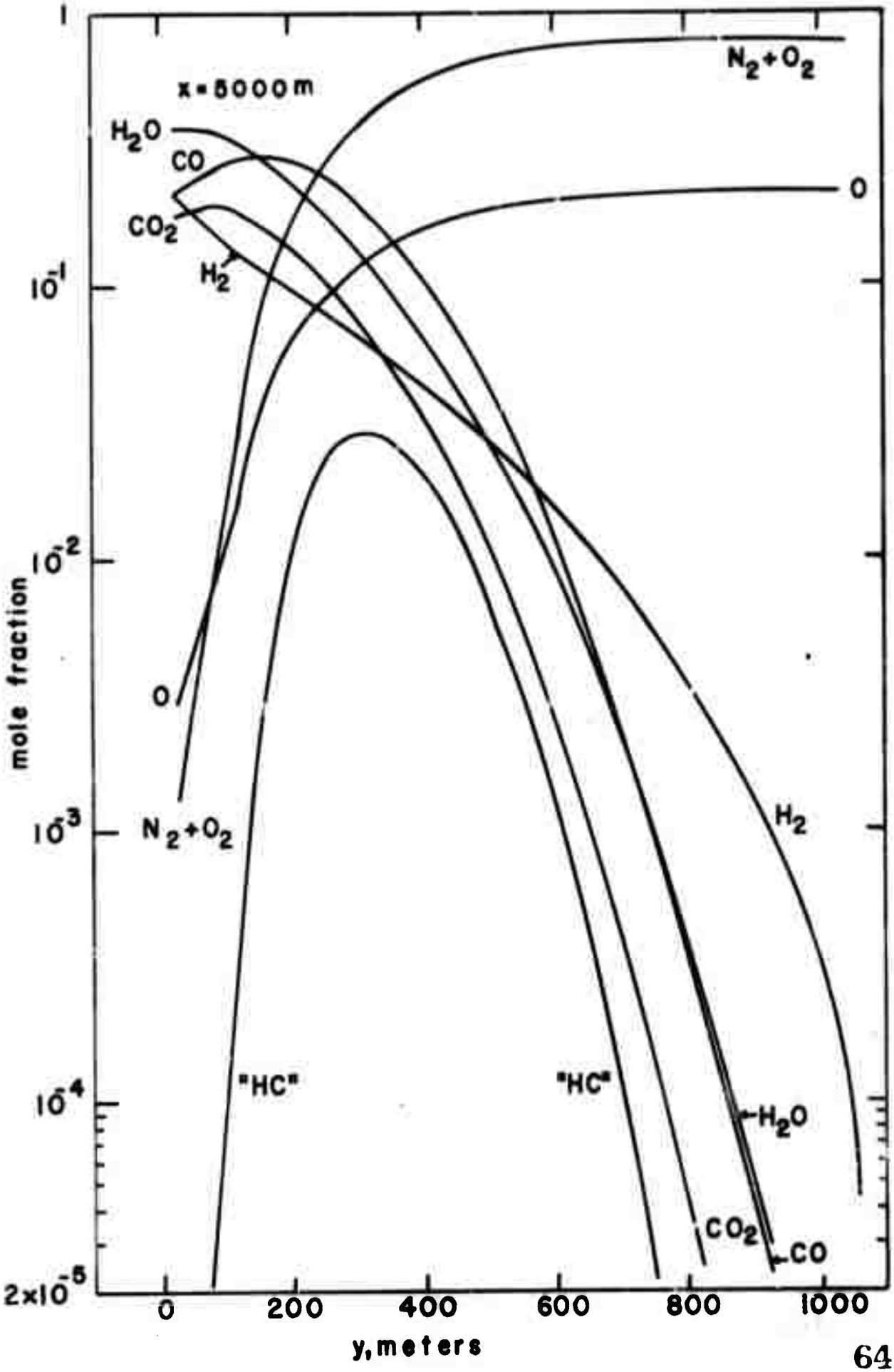
x = 5000 m
N_2+O_2
H_2O
CO
CO_2
H_2
O
10^{-1}
10^{-2}
10^{-3}
10^{-4}
2×10^{-5}
mole fraction
"HC"
"HC"
H_2
H_2O
CO_2
CO
0
200
400
600
800
1000
y, meters

Fig. 25

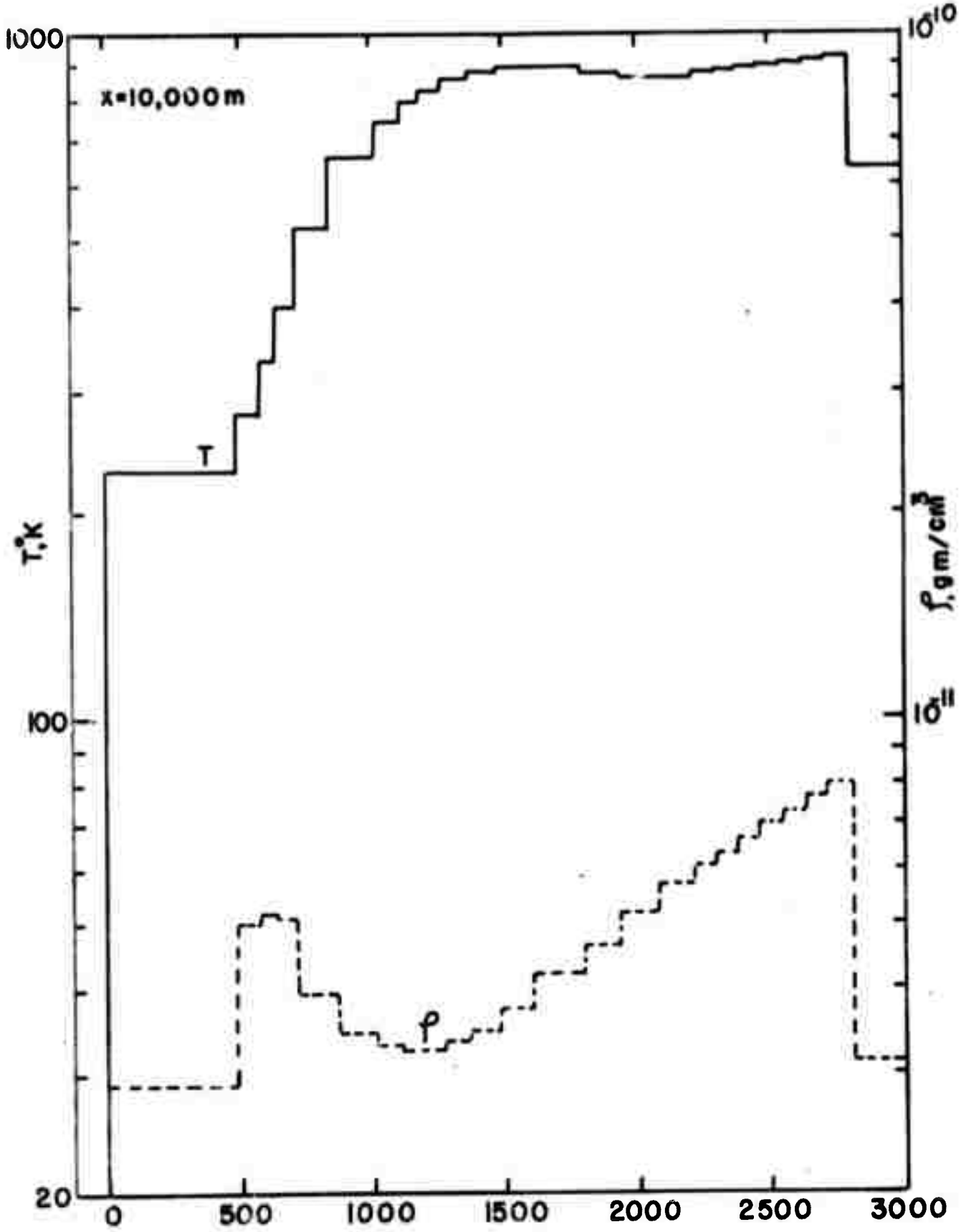
1000
100
20
x=10,000m
T
ρ
T,°K
ρ, gm/cm³
10¹⁰
10¹¹
0
500
1000
1500
2000
2500
3000
y, meters

Fig. 26

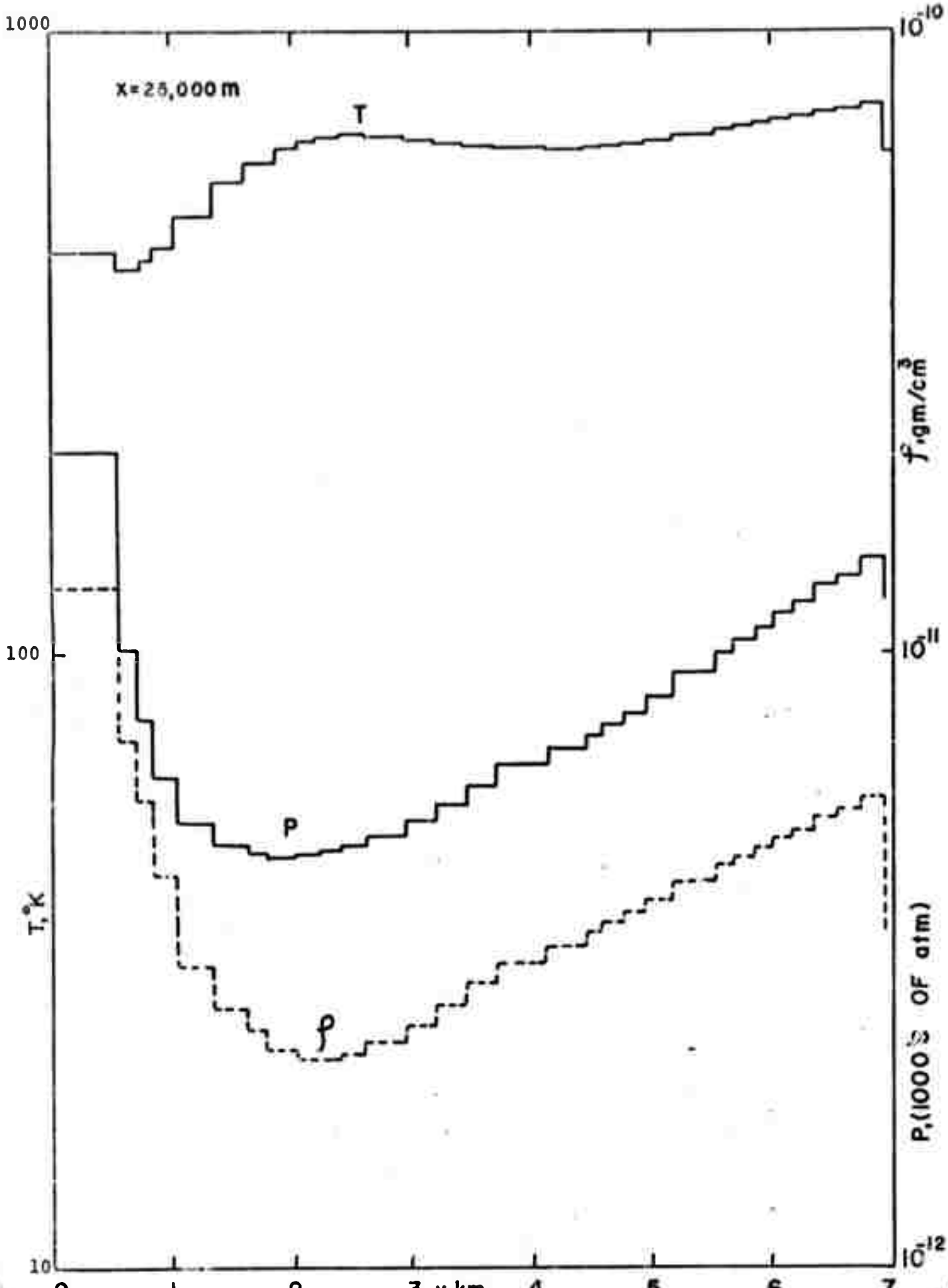
1000
100
10
x=25,000 m
T
P
ρ
T, °K
10^{-10}
10^{-11}
10^{-12}
ρ, gm/cm³
P, (1000's OF atm)
0
1
2
3 y, km
4
5
6
7

Fig. 27

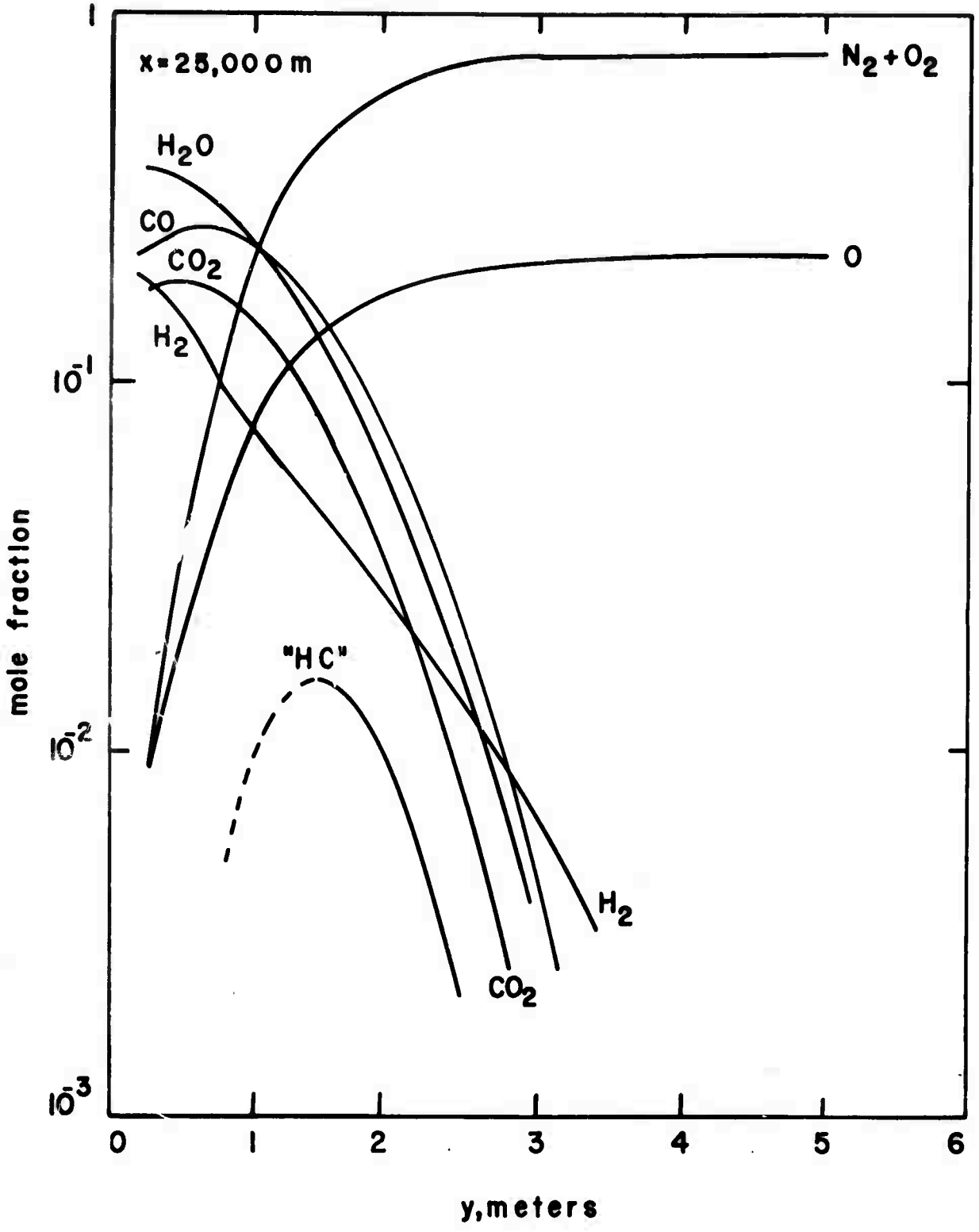
x=25,000 m
N_2+O_2
H_2O
CO
CO_2
H_2
O
"HC"
H_2
CO_2
mole fraction
1
10^{-1}
10^{-2}
10^{-3}
0
1
2
3
4
5
6
y, meters

Fig. 28

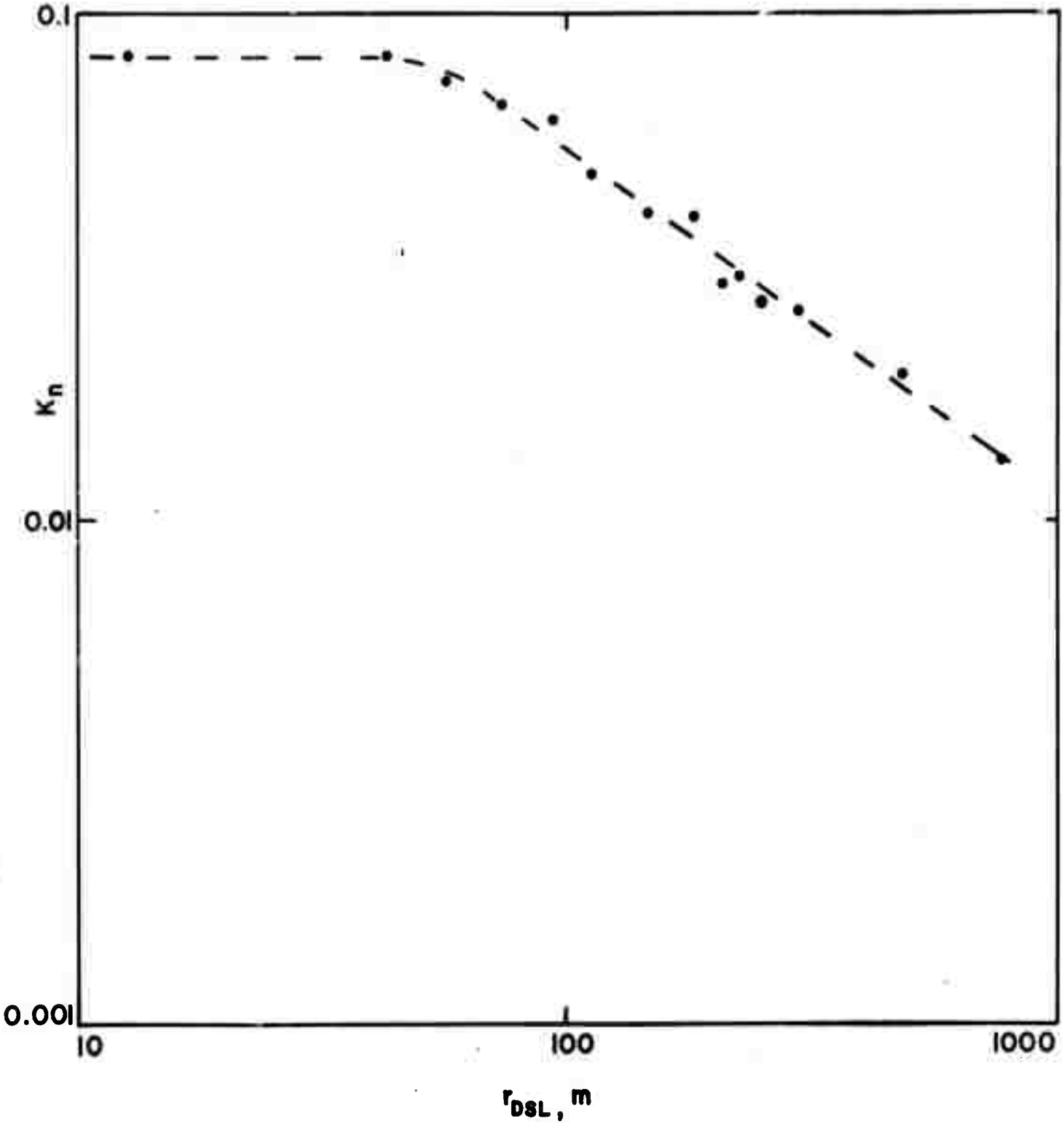

Fig. 29